Geoheritage (2025) 17:168
https://doi.org/10.1007/s12371-025-01219-w

ORIGINAL ARTICLE

Preventive conservation of amber: some preliminary investigations. Pyrite Decay in Amber: Deterioration of Collections and Conservation Guidelines

Rafael Pablo Lozano[1] · Rafael López Del Valle[2] · Eleuterio Baeza[1] · Graciela Delvene[1] · Eduardo Barrón[1] · Enrique Peñalver[1] · Ana Rodrigo[1] · Ricardo Pérez-de la Fuente[3]

Received: 10 January 2025 / Accepted: 11 November 2025

Abstract

Fossilised plant resin (amber) collections represent invaluable sources of information about the past. However, amber is particularly sensitive to exposure to light and oxygen, as well as changing temperature and humidity, rendering its preservation a major challenge. Here we reveal significant degradation of raw and carved amber specimens from part of the Early Cretaceous amber collection of Rábago-El Soplao (Cantabria, Spain), extracted more than a decade ago. These amber specimens, which originated from resin namely formed under subaerial conditions and so generally lack bioinclusions, are of remarkable importance from the palaeoecological, taphonomic, and physicochemical standpoint. Deterioration in amber pieces is due to pyrite decay resulting from the oxidation and hydration of iron sulphides in sedimentary rock remains intimately associated with the amber. We structurally, chemically and morphologically characterise hydrated-sulphate efflorescences found adhered on or included in amber as thin veins or nodules. Clays from sedimentary rock remains associated with the amber play a dual role: they react with acid derived from the dissolution of previous pyrite or sulphates to provide Al, Si, and K that are incorporated into the new sulphates, and they reinforce the alteration of pyrite by hygroscopically capturing water. We also provide guidelines for preventing and remedying pyrite disease in amber specimens, including treatment for new specimens entering collections, optimal physicochemical conditions for storage, and conservation for mildly-altered specimens. Our results urge putting measures in place to guarantee the integrity of the raw and polished amber pieces from the Rábago-El Soplao collection, and are more broadly relevant for the conservation of amber in palaeontological, mineralogical, gemological, and archaeological contexts.

Keywords Sulphide · Pyrite · Movable palaeontological heritage · El Soplao amber · Conservation

Introduction

Amber is fossilised resin produced by trees and other plants. Resins can originate from different botanical species and over time transform into natural polymers with distinct chemical characteristics depending on the type of resin-producing plant species, the physicochemical conditions of the diagenesis, and the elapsed time. Due to their organic nature, amber specimens in museum collections are highly sensitive to deterioration (Girard et al. 2012). As soon as amber is unearthed, degradation begins due to exposure to light, atmospheric oxygen, and fluctuations in both temperature (T) and relative humidity (RH) (Bisulca et al. 2012). The initial stages of such alteration encompass colour change (namely darkening) and cracking at the surface level (Waddington and Fenn 1998; Bisulca et al. 2012).

Regarding light, ultraviolet (UV) is the most harmful part of the spectrum for amber. Prolonged exposure to high levels of UV radiation causes darkening on amber surfaces due to the destruction of C-C bonds (Williams et al. 1990) together with the formation of dark-coloured quinones

✉ Rafael Pablo Lozano
r.lozano@igme.es

[1] Museo Geominero, CN Instituto Geológico y Minero de España (IGME, CSIC), Ríos Rosas 23, Madrid 28003, Spain

[2] Museo de Ciencias Naturales de Álava, Siervas de Jesús 24, Vitoria- Gasteiz 01001, Spain

[3] Oxford University Museum of Natural History, Oxford, UK

Published online: 21 November 2025

(Heinrichs et al. 2013). Along with the action of light, surface cracking occurs due to the interaction with atmospheric oxygen, which causes the oxidation of the amber surface (Waddington and Fenn 1998). Oxidative radical reactions break the polylabdanoid chains, causing depolymerisation of the external surface of the amber (Pastorelli et al. 2013). Although amber surface darkening can be mitigated by filtering UV radiation, keeping specimens in complete darkness is the most effective way to avoid this deterioration (Pastorelli et al. 2011). Preventing contact with oxygen is more challenging to achieve, with solutions involving placing the specimen in an anoxic environment, the most widespread options for which is embedding it in epoxy resin (Sadowski et al. 2021) or placing it inside nitrogen-filled "balloons" (Hansen 1998; Tacker 2020).

Once amber is extracted from the field and set in a museum environment, its rate of deterioration is minimised within certain ranges of T and RH. These optimal ranges vary depending on the locality of provenance and age of the material. In general, amber does not tolerate excessively high or low RH, with the optimal range being between 35 and 60% (Williams et al. 1990; Howie 1995; Thickett et al. 1995). The same applies to T, where the optimal range is between 16 and 25 °C (Williams et al. 1990; Thickett et al. 1995). Outside these ranges, the most damaging effects of these two variables are rapid and repeated fluctuations, with recommendations of not exceeding 2 °C in T and 4% in RH in daily variations (Baeza et al. 2007).

The oxidation/hydration of iron sulphide (pyrite or marcasite), also referred to by the curatorial community as "pyrite disease, decay, or decomposition", is well known as one of the main factors in fossil deterioration due to the widespread presence of iron sulphide (Tacker 2020). Although amber can contain pyrite inclusions (e.g., Martín-González et al. 2009; Hartl et al. 2015; Seyfullah and Schmidt 2015; Álvarez-Parra et al. 2021), and thus this can be an important factor in the deterioration of collections, only partial assessments on these destructive processes in amber have been hitherto conducted (Baeza et al. 2007; Sadowski et al. 2021).

The oxidation of sulphide in the presence of water and atmospheric oxygen produces efflorescent minerals (usually hydrated iron sulphates) and acid. Thus, deterioration of specimens results from the chemical action of this acid or, more worryingly, from the mechanical action resulting from the increase in molar volume. Indeed, as the volume of sulphates is several times greater than the initial volume of the sulphide, their growth produces cracking that can result in the disintegration of the specimens (Becherini et al. 2018). Values of 60% RH are enough for sulphide oxidation to cause deterioration in amber (Sadowski et al. 2021) and other fossils (Larkin 2011). In the case of the latter, remediation consists of mechanical cleaning to remove the efflorescences, chemical intervention to neutralise the acid, and final consolidation (Larkin 2011; Hellemond 2019).

The Rábago-El Soplao amber outcrop formed during the middle Albian (Early Cretaceous) in a restricted tidal channel with low circulation and anoxic water at the bottom. In this palaeoenvironment, a widespread process of early pyritisation occurred (Najarro et al. 2010). In fact, iron sulphide is very abundant and can be found as nodules within the sedimentary rock, replacing mollusc shells (usually gastropods and bivalves), and also in contact with amber and lignite (Najarro et al. 2009). Pyritisation has also been reported in El Soplao in the form of internal marcasite moulds of serpulid worm tubes (Najarro et al. 2010).

In this work, we address the deterioration of part of the Cretaceous amber collection from the Rábago-El Soplao site (Cantabria, Spain) caused by the oxidation/hydration of pyrite found in the rock both adhered to the amber specimens and also present within them. We assess the textural relationship between the pyrite, the sedimentary rock remains, and the amber in order to establish the condition of the sulphide before its alteration. Then we evaluate the environmental causes of the deterioration and the role of the sedimentary rock remains adhered on or included in the amber during the alteration process of the pyrite with the incorporation of chemical elements into the neoformed hydrated sulphates, derived from clay minerals. Preventive and remedial recommendations for the conservation of amber collections from pyrite decay are provided.

The Rábago-El Soplao Site and its Scientific Relevance

The amber deposit of Rábago-El Soplao is located in the municipality of Rábago, within the "El Soplao territory" (Cantabria, north Spain). The site was discovered in the roadside ditch of the access road to the El Soplao tourist cave, where an Albian siliciclastic unit outcrops (Najarro et al. 2009). The abundance of amber in this deposit is unusually high when compared to other Spanish amber sites (Najarro et al. 2010).

Most of the amber consists of large kidney-shaped pieces (up to 25 cm in length) that were formed under subaerial conditions (by the roots or in tree pockets), and only a small part is stalactite-shaped, corresponding to resin that was produced in exposed, aerial conditions and often having morphologies that followed a gravity gradient (Najarro et al. 2009, 2010). Although no bioinclusions have been hitherto found in the kidney-shaped specimens, they provide vital

palaeoecological, taphonomic, and physicochemical information. Whereas kidney-shaped amber specimens commonly show a thick crust of opaque, altered (milky coffer brown in colour) amber due to the colonisation of resinocolous fungal hyphae, aerial amber is generally not affected by fungal activity, (Speranza et al. 2015). Kidney-shaped specimens have also been used to study the organic chemical composition of the amber (Menor-Salván et al. 2009, 2010, 2016) and its physical properties (Pérez-Castañeda et al. 2014). Moreover, this type of amber was used to characterise fossilised sap; this plant substance is found in the form of vacuolar pseudoinclusions, which actually constitute double resin-in-sap-in-resin emulsions (Lozano et al. 2020).

The stalactite-shaped specimens usually contain arthropod bioinclusions (Najarro et al. 2010), which have led to notable scientific production. Some of the fossil arthropods described encompass insects such as barklice (Psocoptera) (Álvarez-Parra et al. 2023), midges, mosquitoes and flies (Diptera) (Pérez-de la Fuente et al. 2011; Arillo et al. 2015, 2018; Lukashevich and Arillo 2016), scorpioflies (Mecoptera) (Soszyńska-Maj et al. 2022), wasps (Hymenoptera) (Peñalver et al. 2010; Ortega Blanco et al. 2011a, 2011b; Pérez-de la Fuente et al. 2012a), snakeflies (Raphidioptera) (Pérez-de la Fuente et al. 2012b), lacewings (Neuroptera) (Pérez-de la Fuente and Peñalver 2019; Pérez-de la Fuente et al. 2021), beetles (Coleoptera) (Peris et al. 2014), as well as arachnids, both spiders (Araneae) (Saupe et al. 2011; Pérez-de la Fuente et al. 2013) and mites (Acari) (Arillo et al. 2016). Other works on Rábago-El Soplao amber focus on ecological processes and biotic interations that occurred during the Cretaceous, such as pollination (Peñalver et al. 2015; Peris et al. 2017), camouflage (Pérez-de la Fuente et al. 2016), parasitism (Arillo et al. 2018), or resin consumption by resinicolous fungi forming crusts (Speranza et al. 2015). All the specimens from this amber locality are housed in a unique institutional collection protected under the heritage laws of the Cantabrian Autonomous Community (law 11/1998, Cultural Heritage; Decree 36/2001: Partial development of the 11/98, Cantabrian cultural heritage law; Law 5/2001, on museums of Cantabria; register of museums and collections of Cantabria). Its abundant and diverse palaeontological content demonstrates the high scientific and heritage importance of the Rábago-El Soplao amber collection.

The Amber Collection

Most of the specimens were obtained during four palaeontological excavations carried out to date, between 2008 and 2010. Additionally, some of the material was gathered on the surface of the site after the rainy season. The total amount of amber extracted (excavations + surface collections) is estimated to be around 80 kg, of which approximately 40% has been processed. Processing includes a thorough examination of each amber piece in search of bioinclusions as well as to detect surface features (impressions, encrusted fossils…) of interest. It also includes the preparation of the bioinclusions for palaeozoological and palaeobotanical research.

To date, the amber collection consists of 1023 specimens and is composed of three sub-collections:

1. *Preparations with bioinclusions*. This sub-collection consists of 876 preparations, each with at least one bioinclusion. The vast majority are embedded in epoxy resin (EPO-TEK 301), and only 10 specimens are not embedded due to their morphological interest or the peculiarities of the bioinclusions. The total number of bioinclusions is 1490, mostly corresponding to arthropods, and, to a lesser extent, plants, fungi, and feather remains. In the short term, the amber embedded in epoxy resin is not susceptible to alteration, and only the unembedded specimens may be prone to preservation issues.
2. *Raw specimens*. This sub-collection comprises 119 specimens. These are samples selected for their notable interest due to their origin (kidney-shaped or stalactite-shaped pieces), surface marks, fossils adhered on surfaces, or peculiar inclusions (such as fragments of fossil wood, i.e., lignite). In the short term, this collection is highly susceptible to deterioration given the presence of remains of pyrite-rich rock in many specimens. Approximately 10% of the specimens show efflorescences visible to the naked eye.
3. *Polished specimens*. This sub-collection consists of 37 specimens, including polished pieces of various morphologies, sections (specimens with polished flat surfaces), and faceted samples. In order to carve the amber without breaking it, applying synthetic resins (epoxy or polyester) under vacuum was necessary due to the original fracturing of the raw specimens. In the short term, this collection is also susceptible to deterioration for the same reason as the previous one. Although the specimens do not show efflorescences visible to the naked eye, some have cracked.

Although the present work focuses on the raw and polished amber specimens, the results have also implications for the mid to long-term management of the more stable amber preparations with bioinclusions.

Environmental Conditions

Cantabria, the region where the outcrop and collection are located, is a Spanish autonomous community and province with a cool summer humid temperate climate, predominantly influenced by the Atlantic (the average annual precipitation exceeds 1200 mm and the average annual RH exceeds 75%; data from the Spanish Meteorological Agency, AEMET). Most of the Rábago-El Soplao amber material is stored in a room belonging to the Government of Cantabria, located next to the entrance of the El Soplao Cave (550 m above sea level), just a few kilometres from the Rábago-El Soplao amber deposit (Sierra de Arnero, northern slope of the Cantabrian Mountains, northern Spain), with an average annual T of 11.3 °C (the cave's internal T reflects well the average external T; Rossi et al. 2018).

The room where the amber is stored is small (2.1×4.3×2.6 m) and was not originally designed for preserving collections, so the environmental conditions are not ideal. Additionally, this space is also used as a workshop for preparing bioinclusions by one of us (R.L.D.V.). The room is not completely airtight and is therefore influenced by external RH variations. The amber has been stored in this room since 2009, when an electric dehumidifier was installed aimed to reduce the RH in the room. This dehumidifier broke down two years later and was replaced by a second dehumidifier, which is currently operating (ORBEGOZO DH-2050). Following turnover in the Government of Cantabria in 2012, the contract of the collection's curator (R.L.D.V.) was terminated, and the collection was without curation until being rehired in 2022, coinciding with another political change. Currently, the lower T limit is set at 18 °C (the average T is around 20 °C), although the RH, with the dehumidifier in operation, never drops below 60%. For example, on the rainy morning of 1 August 2024, the RH inside the room was 79% at 25 °C despite the dehumidifier was running at full capacity.

Fig. 1 Public exhibition on Rábago-El Soplao amber at the visitor facilities next to El Soplao Cave (photographs taken in 2024) (**a**) Overview of the exhibition located in the service rooms from the El Soplao Cave visitors, nearby the storage room. Individual displays shown in other subfigures have been marked. (**b**) Detail of a preparation in epoxy resin with multiple bioinclusions. (**c**) Set of six polished amber specimens. (**d**) Raw amber specimen with clear signs of deterioration due to pyrite decay

A small part of the collection is on public exhibition in close proximity to the storage room, in the service rooms for visitors to the cave (Fig. 1a). In this small exhibition, lacking any atmospheric control measures, a preparation with bioinclusions (Fig. 1b), six polished specimens (Fig. 1c) and three raw specimens are displayed. One of the latter shows clear external signs of deterioration (Fig. 1d).

Methodology

Table 1 shows the list of samples analysed, including the type of sample and analysis, and their location within the figures.

The analyses of sulphur and hydrated sulphates in the Rábago-El Soplao amber have been carried out via powder X-ray diffraction (XRD) using a X'Pert PRO apparatus (Panalytical) with a copper tube, a graphite monochromator and automatic divergence slit at the Centro Nacional - Instituto Geológico y Minero de España, Consejo Superior de Investigaciones Científicas (IGME, CSIC, Tres Cantos, Madrid) facilities. Identifications were made using X'Pert High Score software by Panalytical and the PDF-2 (ICDD) database.

Table 1 List of samples analysed, including the type of sample and analysis, and their location within the figures

Sample	Description	XRD	SEM + EDX	Figures
SO-1	Efflorescence	Yes	No	
SO-2	Efflorescence	Yes	No	
SO-3	Raw amber with efflorescence in pyrite-rich rock	Yes	Yes	7a
SO-4	Unaltered pyrite-rich rock	Yes	Yes	2c, d; 7f
SO-5	Raw amber with efflorescence on the surface	Yes	Yes	7b, c; 11d
SO-6	Raw amber with efflorescence on the surface	Yes	Yes	7e; 11b, c
SO-7	Raw amber with efflorescence in pyrite-rich rock	Yes	Yes	3f; 10c, d
SO-8	Raw amber with efflorescence in pyrite-rich rock	Yes	Yes	7d; 9; 11a; 12
SO-9	Raw amber with efflorescence in pyrite-rich rock	Yes	Yes	
SO-10	Raw amber with efflorescence in pyrite-rich rock	Yes	No	
SO-11	Polished amber with efflorescence in pyrite-rich rock	No	Yes	3a-e; 10a, b

Ten samples (SO-1 to SO-10) were analysed using XRD. Samples SO-1 and SO-2 correspond to undifferentiated efflorescences collected from the bottom of the cardboard boxes where the amber specimens are stored. Sample SO-4 corresponds to an aggregate of sedimentary rock rich in sulphide seemingly unaltered (without efflorescences visible to the naked eye) and which was adhered to the surface of an amber specimen. The remaining samples were obtained by scraping the efflorescences with a scalpel. Except for SO-4, all samples were manually purified using a binocular microscope to remove as much sulphide as possible.

Carbon coated surfaces of samples were observed using JSM-6010 PLUS/LA scanning electron microscope (SEM) equipped with an energy-dispersive X-ray microanalyser (EDX) and a secondary electron detector (SE) at the CN-IGME, CSIC facilities (Tres Cantos, Madrid). The chemical composition was estimated using the standardless quantification method implemented in the JEOL analysis software, which calculates elemental concentrations from relative X-ray peak intensities applying ZAF (atomic number, absorption, and fluorescence) matrix corrections. The results are reported as semi-quantitative values, normalised to 100% of the detected elements. The vacuum in the SEM specimen chamber is 0.01 Pa. The samples were coated using a Cressington 108 carbon coater under a vacuum of 15 Pa.

This technique was also used to study a sample of polished amber with veins of sulphide-rich rock (SO-11) and a sample with sulphide-rich nodules (SO-7). Additionally, surfaces of amber with hydrated sulphates (samples SO-5 and SO-6) and surfaces of sulphide-rich rock remains adhered to amber, partially altered to hydrated sulphates (SO-3, SO-8, and SO-9), were studied with SEM. In sample SO-4 and SO-8, freshly broken surfaces of the sulphide-rich rock were examined.

Some photographs were taken with a Canon EOS 650D digital camera using Macrofotografía version 1.1.0.5 (CN-IGME, CSIC, Madrid, Spain), which integrates the Helicon Focus software to create composite photographs by stacking sequential images taken at different focal planes.

Photography was enhanced in Photoshop CC 2020 for adjust brightness and contrast, and composite figures were prepared using CorelDRAW X8 software.

Two Cretaceous amber fragments, each containing bioinclusions and pyrite and embedded in epoxy resin (EPO-TEK 301)—one originating from Rábago-El Soplao (sample 495) and the other from Peñacerrada, Álava, Spain (sample 9935)—were examined using a binocular microscope.

Results

Textural Relationship Between Pyrite and Amber

In Rábago-El Soplao amber specimens, pyrite is associated with clayey-sandy rock, forming aggregates of equidimensional crystals of sizes ranging between 20 and 500 µm. The rock-pyrite assemblage is adhered onto the surface of the amber specimens (Fig. 2) and/or included within the amber (Fig. 3). In both cases, the amber in contact with the pyrite-rich rock has the characteristic opaque milky coffee brown colour of fungi-altered amber (Cretaceous alteration). Sample SO-4 is an unaltered pyrite-rich rock adhered to the amber surface to it XRD indicates that the sulphide is pyrite, not marcasite. Detailed SEM examination of the broken surfaces of this sample shows trapezohedral pyrite crystals included in the rock portion (clay minerals + quartz; Fig. 2c, d). There is a silicate patina between the pyrite crystals and the clay matrix (Fig. 2d).

Pyrite (or pyrite-rich rock) is also found within amber pieces altered by fungi in the form of thin veins (sample SO-11; Fig. 3a) or small nodules (Fig. 3f). Under long-wave ultraviolet light, the altered amber does not show the typical blue fluorescence of unaltered amber, as much of the

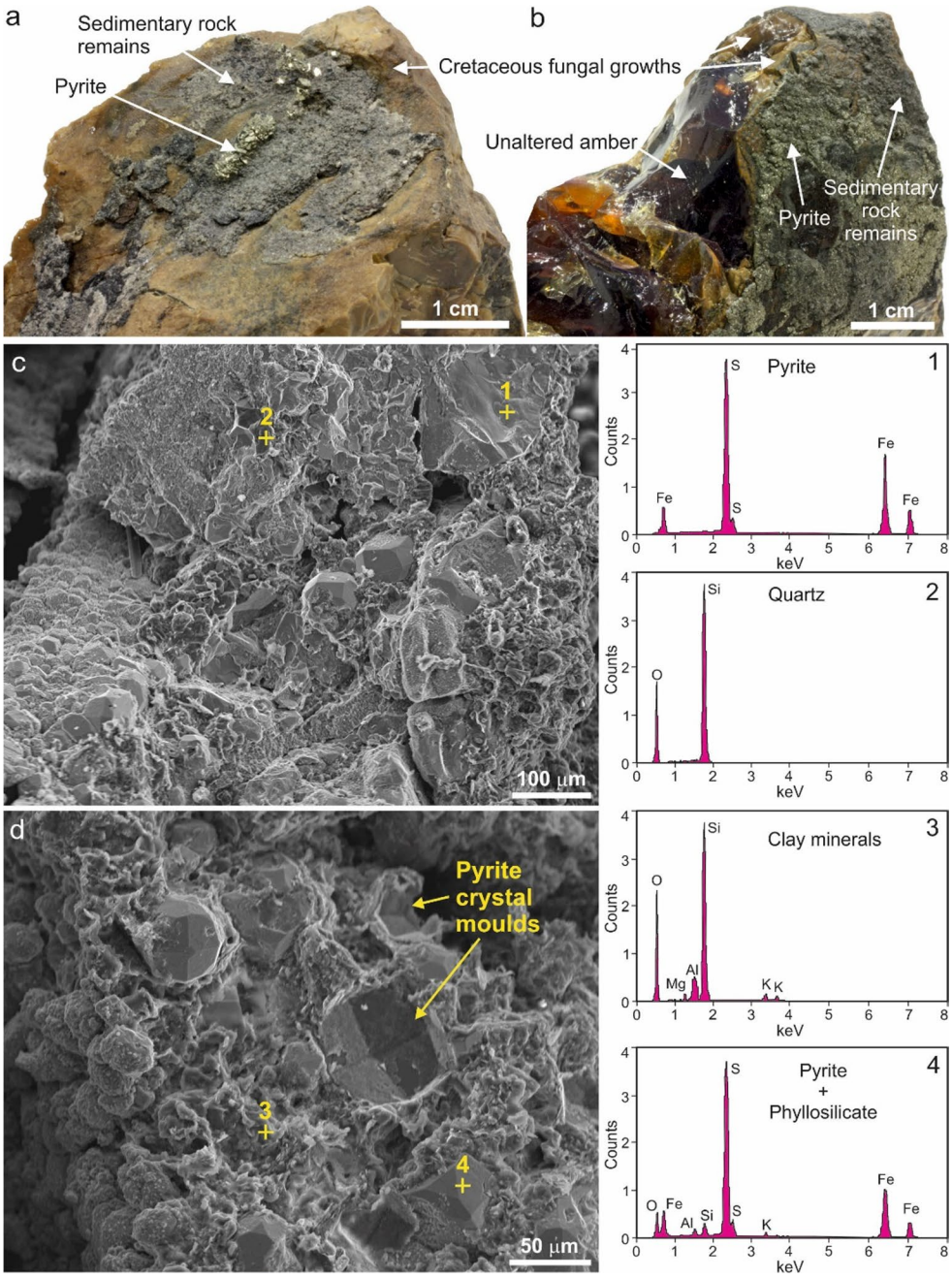

Fig. 2 Characterization of rock-pyrite assemblage adhered to the external surface of amber specimens from Rábago-El Soplao. (**a**–**b**) Two amber specimens photographed in 2010 and currently destroyed due to pyrite alteration. Both specimens have a crust due to resinicolous fungal mycelia that grew during the Cretaceous (brown milk-coffee colour). (**c**–**d**) SEM images (backscattered electrons) of the interior of the pyrite-rich remains of rock (broken surfaces) adhered on amber specimen (sample SO-4). EDX spot chemical analyses of areas of interest are shown. Inside the sample, the pyrite remains unoxidised and lacking hydrated sulphate growth. (**c**) Trapezohedral pyrite crystals embedded in clay minerals (central area of the image). Analysis 1 corresponds to the broken surface of a pyrite crystal; analysis 2 to a quartz grain. (**d**) Different area of the same sample where trapezohedral pyrite crystals are observed. Analysis 3 corresponds to clay minerals containing Al, K, and some Mg, in addition to Si and O; analysis 4 corresponds to the surface of a pyrite crystal. In addition to S and Fe, Si, O, Al, and traces of K are systematically present, which is interpreted as a nanometric silicate-rich patina. In the central area of the image, two moulds are visible, formed after the sample broke away from a pyrite crystal. This film, partially detached, can be observed on the surface of the moulds

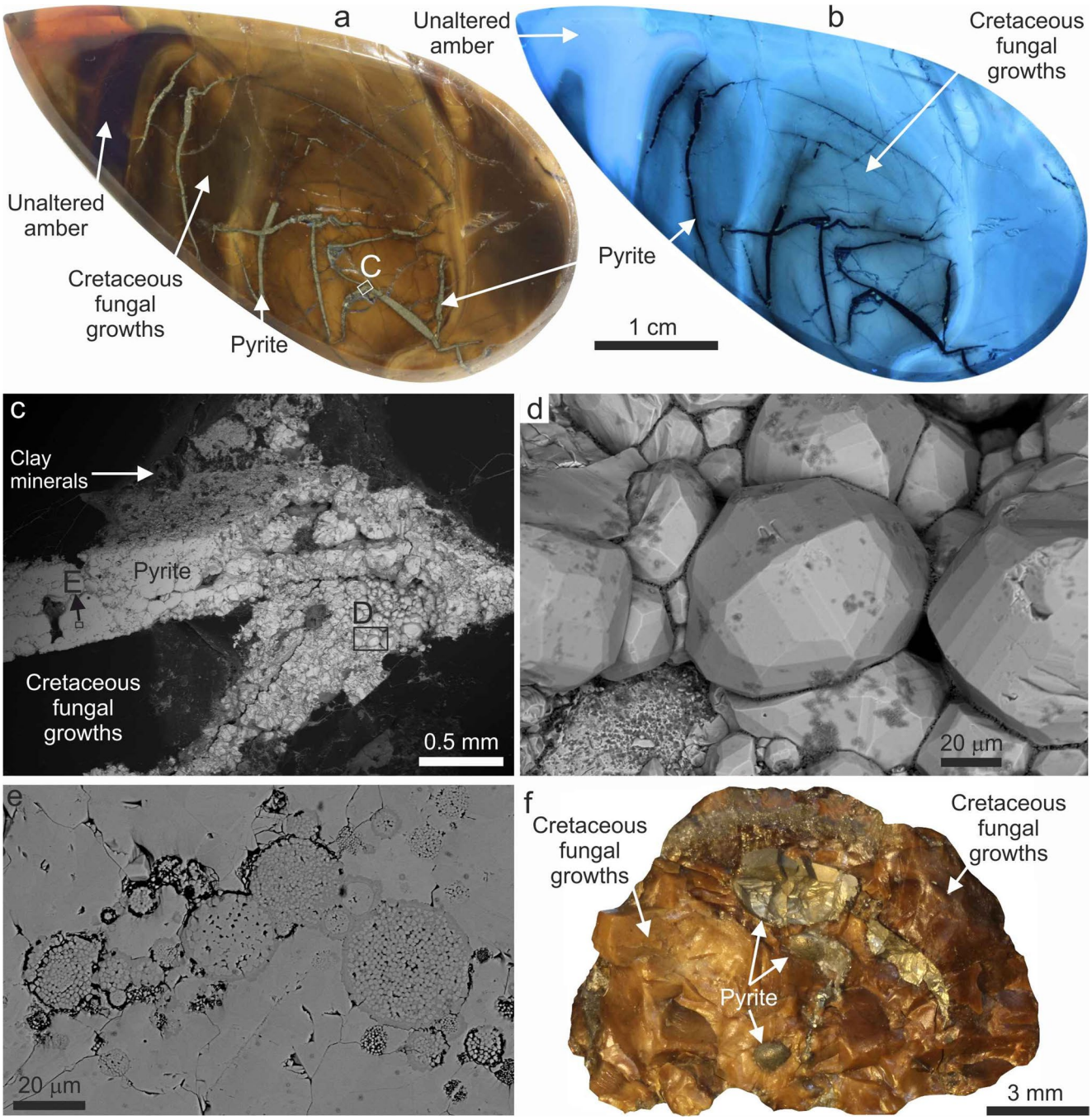

Fig. 3 Characterization of rock-pyrite assemblage included within amber specimens from Rábago-El Soplao. (**a**–**b**) Polished amber specimen (sample SO-11) showing the relationship between fungus-altered amber and thin pyrite-filled veins (pyrite-rich rock). Image (**a**) was taken under visible light, and (**b**) under long-wave ultraviolet light (note the decrease in fluorescence in areas partially altered by the Cretaceous fungi). (**c**) Detail from (**a**) of a pyrite-filled vein with sedimentary rock. (**d**) Detail from (**c**) of a cavity lined with pyrite crystals, exhibiting their crystalline morphology (complex form with a trapezohedral tendency). (**e**) Detail from (**c**) of the aggregation of framboidal pyrite within the massive pyrite vein. (**c**–**e**) are SEM images (back-scattered electrons). (**f**) Appearance of amber specimen (sample SO-7) completely altered by Cretaceous fungi with pyrite-rich rock nodules embedded. Image obtained by stacking multiple images taken at different focal depths

original resin was consumed during fungal colonisation (Fig. 3b). Some of these small veins are not completely filled and show the crystalline morphology of the pyrite, usually more complex than the typical trapezohedral crystals (Fig. 3d). Within the vein pyrite, small pyrite framboids are preserved, with minute individual crystals that are 0.5 to 1 µm (Fig. 3e).

In aerial specimens, remnants of pyrite-rich rock are typically found adhered to unaltered (transparent) amber rather than altered (opaque) amber. Additionally, some of these adhered rock remnants include pyritised shells of bivalves (Fig. 4a–b) and gastropods (Fig. 4c–d). When pyrite is located within unaltered amber, it is visible through transparency and often forms crystal aggregates (Fig. 4e), and it can even fill the volume of the bioinclusions themselves (Fig. 4f). Normally this pyrite is associated with secondary planes within the amber.

Fig. 5 Raw amber specimens from the collection of Rábago-El Soplao. (**a**) Cardboard box showing smaller sample boxes almost all of which originally contained one amber piece in each. The numerous amber fragments present in many boxes are the result of the disintegration of large specimens due to pyrite oxidation/hydration and sulphate growth. Sulphate efflorescences are evident in samples b–d. (**b**) Acicular and powdery efflorescence on one of the specimens. Note that acid production has deteriorated the base of the cardboard box. (**c**) Thin pyrite-rich rock veins with incipient efflorescence formation. (**d**) Specimen with incipient acicular efflorescences both on its external and breaking surfaces. Sulphate growth within the specimen has caused significant fracturing of the amber. In specimens (**c**) and (**d**), the crust of fungal alteration is present, always associated with remains of pyrite-rich rock

Hydrated-Sulphate Efflorescences

Raw amber specimens are stored in cardboard boxes (Fig. 5a). All the boxes that have been examined contain specimens that are deteriorated to a lesser or greater extent. Some of them

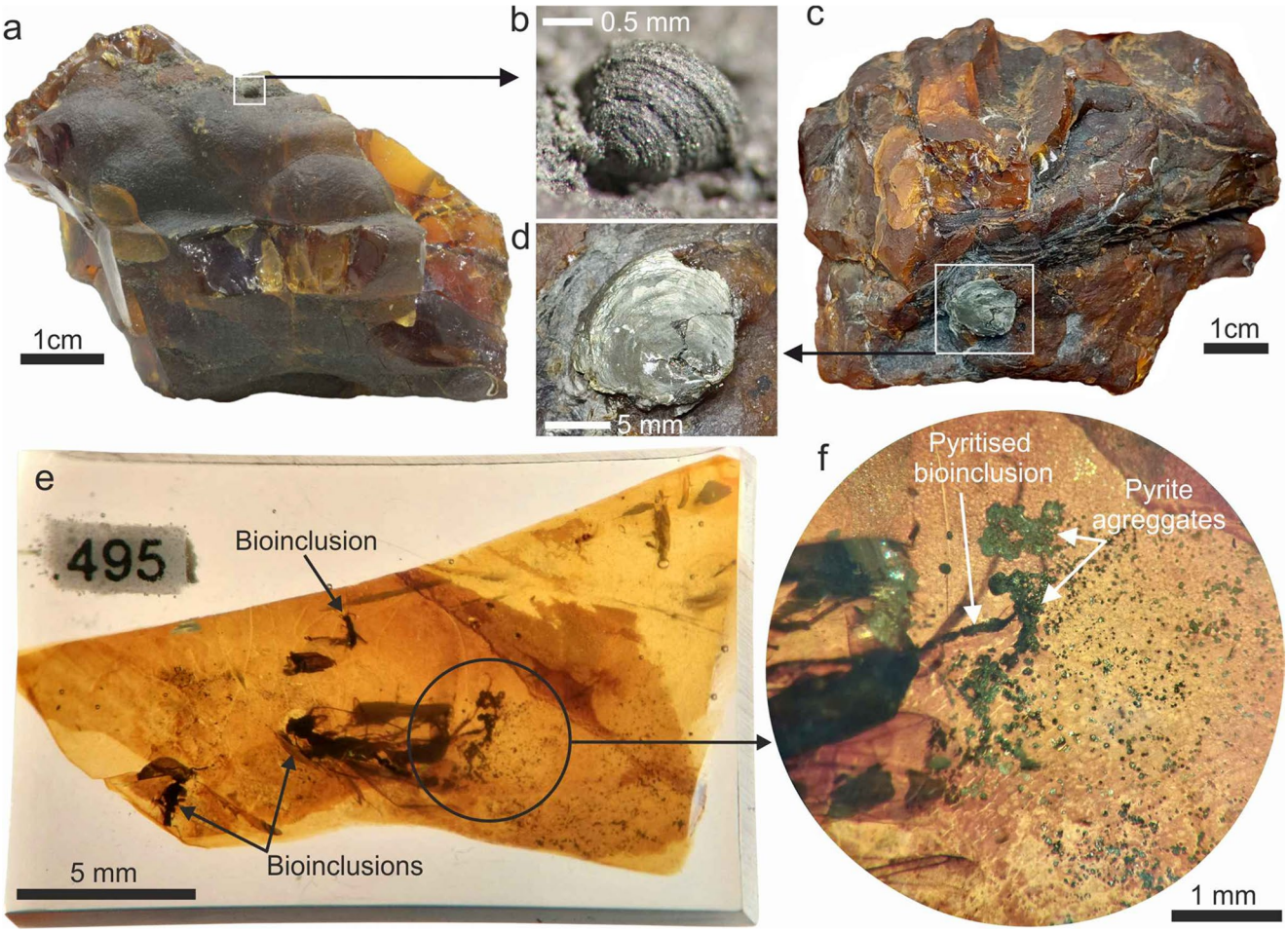

Fig. 4 Rábago-El Soplao amber pieces of the aerial type associated with pyrite. (**a**) Amber specimen (CES 180) with sedimentary rock remains, including a gastropod shell replaced by pyrite. (**b**) Detail of the gastropod shell in (**a**). (**c**) Amber specimen (CES-189) with a bivalve shell (replaced by pyrite) attached to its surface. (**d**) Detail from the bivalve shell in (**c**). (**e**) Amber fragment with bioinclusions embedded in epoxy resin. (**f**) Detail from (**e**) showing pyrite aggregates in a plane affecting one of the bioinclusions. Note that the antenna of one of the fossils is composed of pyrite. Inside the epoxy resin, the pyrite remains unaltered


a
b
c
d
5 cm

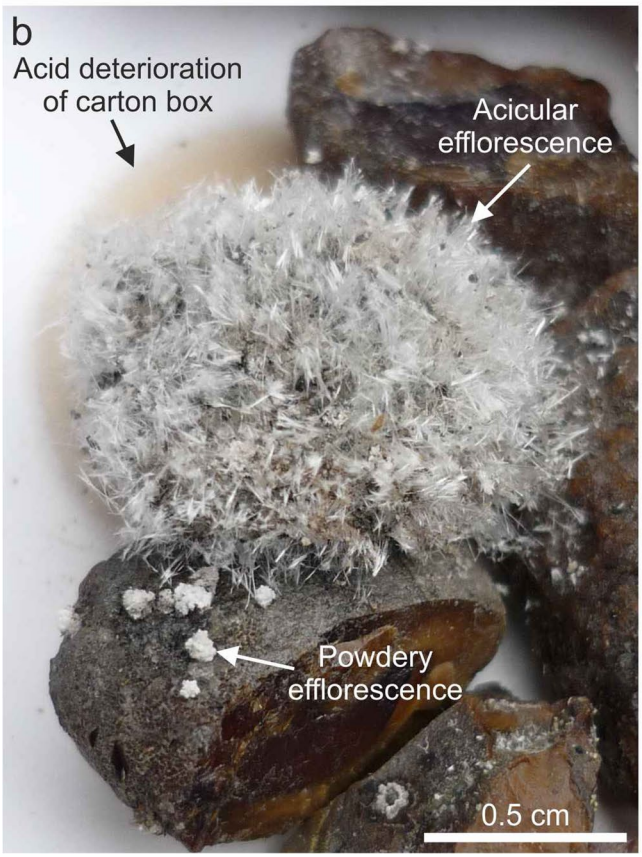
b
Acid deterioration of carton box
Acicular efflorescence
Powdery efflorescence
0.5 cm

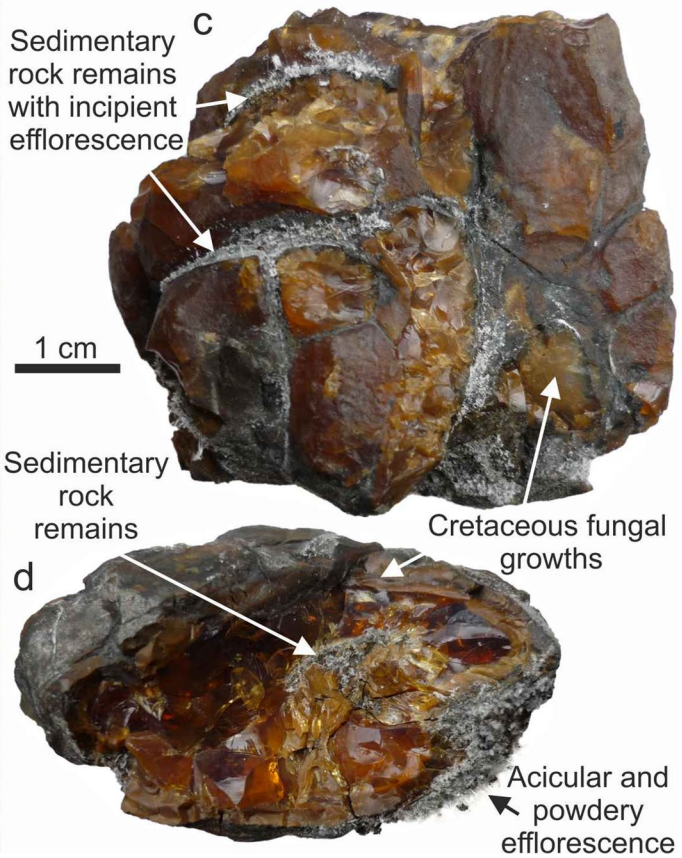
c
Sedimentary rock remains with incipient efflorescence
1 cm
Sedimentary rock remains
Cretaceous fungal growths
d
Acicular and powdery efflorescence

remain unaltered, while others show small, localised efflorescences, at times acicular (Fig. 5b). The efflorescences preferentially grow on the pyrite-rich rock partially or fully embedded in the amber specimens (Fig. 5c, d), although hydrated sulphates also grow directly on the surface of the amber. In some cases, the box cardboard has deteriorated due to exposure to acid resulting from the oxidation/hydration process of the pyrite (Fig. 5b).

A remarkable instance is shown by an amber specimen faceted during 2010 and was extracted from a much larger kidney-shaped piece (Fig. 6a). The amber was commissioned by the Government of Cantabria for the exhibition "The Long Journey of El Soplao Amber", which opened that same year. Fourteen years later, the carved specimen shows a large crack on its main facet, but no visible efflorescences (Fig. 6b).

By combining structural (XRD), chemical (EDX), and morphological (SEM) data, the mineralogical composition of the efflorescences has been determined. They consist of five different hydrated sulphates: halotrichite ($Fe^{2+}Al_2(SO_4)_4 \cdot 22H_2O$), coquimbite ($Fe^{3+}_{2-x}Al_x(SO_4)_3 \cdot 9H_2O$), paracoquimbite ($Fe^{3+}_{2-x}Al_x(SO_4)_3 \cdot 9H_2O$), szomolnokite ($Fe^{2+}SO_4 \cdot H_2O$) and ferricopiapite ($Fe^{3+}_{0.66}Fe^{3+}_4(SO_4)_6(OH)_2 \cdot 20H_2O$) (Fig. 7). Thus, the sulphates containing Fe^{2+} or Fe^{3+}, have different amounts of structural water (from 1 to 22 molecules), and can incorporate only Fe or Fe+Al (with traces of Si and K).

All the samples analysed by XRD (ten samples) contain szomolnokite (+pyrite), which, along with coquimbite (found in eight out of the ten samples), is the most common sulphate (Fig. 8). Halotrichite is found in three samples, paracoquimbite in two samples, and ferricopiapite in only one sample. XRD analysis of sample SO-4 (pyrite-rich rock, presumably unaltered) indicates the presence of pyrite, quartz, szomolnokite, and only trace of phyllosilicates, without species identification. In the SEM study, gypsum was found as accessory in this same sample (Fig. 7f).

SEM+EDX data indicate that halotrichite forms fibrous radial aggregates of white acicular crystals with a fuzzy appearance, up to 3 mm in length and between 1 and 5 µm in thickness (Figs. 5b and 7a). In addition to Fe and Al, these halotrichite aggregates incorporate traces of Si (est. 1–2%wt). Coquimbite and paracoquimbite are two polymorphic phases. Coquimbite forms aggregates of yellow hexagonal tabular crystals (Fig. 7b), morphologically very different from those of paracoquimbite, which forms parallel or radial aggregates of hexagonal prismatic crystals up to 250 µm in length and between 1 and 30 µm in thickness (Fig. 7c). The size of the coquimbite crystals ranges between 5 and 10 µm, although occasionally the coquimbite forms larger skeletal crystals, between 5 and 100 µm. The chemical composition of the two phases is identical, and both incorporate some Si (est. 1–2%wt) and K (est. 1–4%wt). Szomolnokite forms aggregates of small tabular crystals (between 1 and 15 µm); this phase is chemically pure and does not incorporate Al, Si, or K (Fig. 7d). Lastly, ferricopiapite forms rosette-like aggregates of yellow laminated hexagonal crystals (Fig. 7e), ranging in size from 5 to 40 mm. Like szomolnokite, ferricopiapite does not incorporate traces of elements other than those in its crystalline structure.

In amber specimens with thin veins of pyrite-rich rock (sample SO-8), the efflorescences are generated directly on the exposed surfaces of the veins (Fig. 9a), although they can extend to the surfaces of fungus-altered amber (Fig. 9d). The most visible sulphate to the naked eye is halotrichite, which grows on the pyrite-rich rock (Fig. 9b), more specifically in cracks generated in it (Fig. 9c, d). Szomolnokite lines the pyrite crystals and seems to have grown before halotrichite (Fig. 9d, e). Coquimbite also grew early on the pyrite-rich rock (Fig. 9d, f). SEM observations within these veins in other samples (SO-11) revealed abundant framboidal pyrite crystals within the pyrite mass (Fig. 3e). The most fractured sections of the veins have begun to alter to hydrated sulphates, both of Fe and of Fe and Al (Fig. 10a, b).

The pyrite-rich rock nodules found within fungus-altered amber (sample SO-7) also show alteration. The surface of the nodules (nodule-amber interface) is covered by an amorphous sulphate upon which szomolnokite grows (Fig. 10c, d). In some of these nodules, there are phyllosilicate aggregates on which coquimbite crystals have grown, now partially dissolved (Fig. 10c, d).

SEM observations reveal halotrichite fibres and szomolnokite aggregates coating the cracks of pyrite-rich rock (sample SO-8; Fig. 11a). Crystalline aggregates of ferricopiapite and paracoquimbite grow on the surface of fungus-altered amber and within its fractures (samples SO-6 and SO-5; Fig. 11b, c, d).

Sample SO-8 was fragmented to examine the alteration state and internal texture of the fine veins within the pyrite-rich rock. Similar to the exterior, the pyrite within is partially altered to sulphates. The rock contains abundant fossilised remains of pyritised molluscs (gastropods and bivalves) and halotrichite efflorescences visible to the naked eye (Fig. 12a). SEM observations reveal that nearly the entire surface of the shells is coated with szomolnokite (Fig. 12b, c) and, in addition, that halotrichite has grown inside the pyritized molluscs (Fig. 12d).

Curative Procedures

Mechanical cleaning trials were conducted to remove the efflorescences that developed on the pyrite-rich rock and the surface of the amber. The more visible efflorescences (mainly halotrichite) are removed with relative ease using brushes of varying thickness. However, the less visible efflorescences (mainly szomolnokite) are strongly adhered to the surface of the pyrite-rich rock and the amber, rendering their

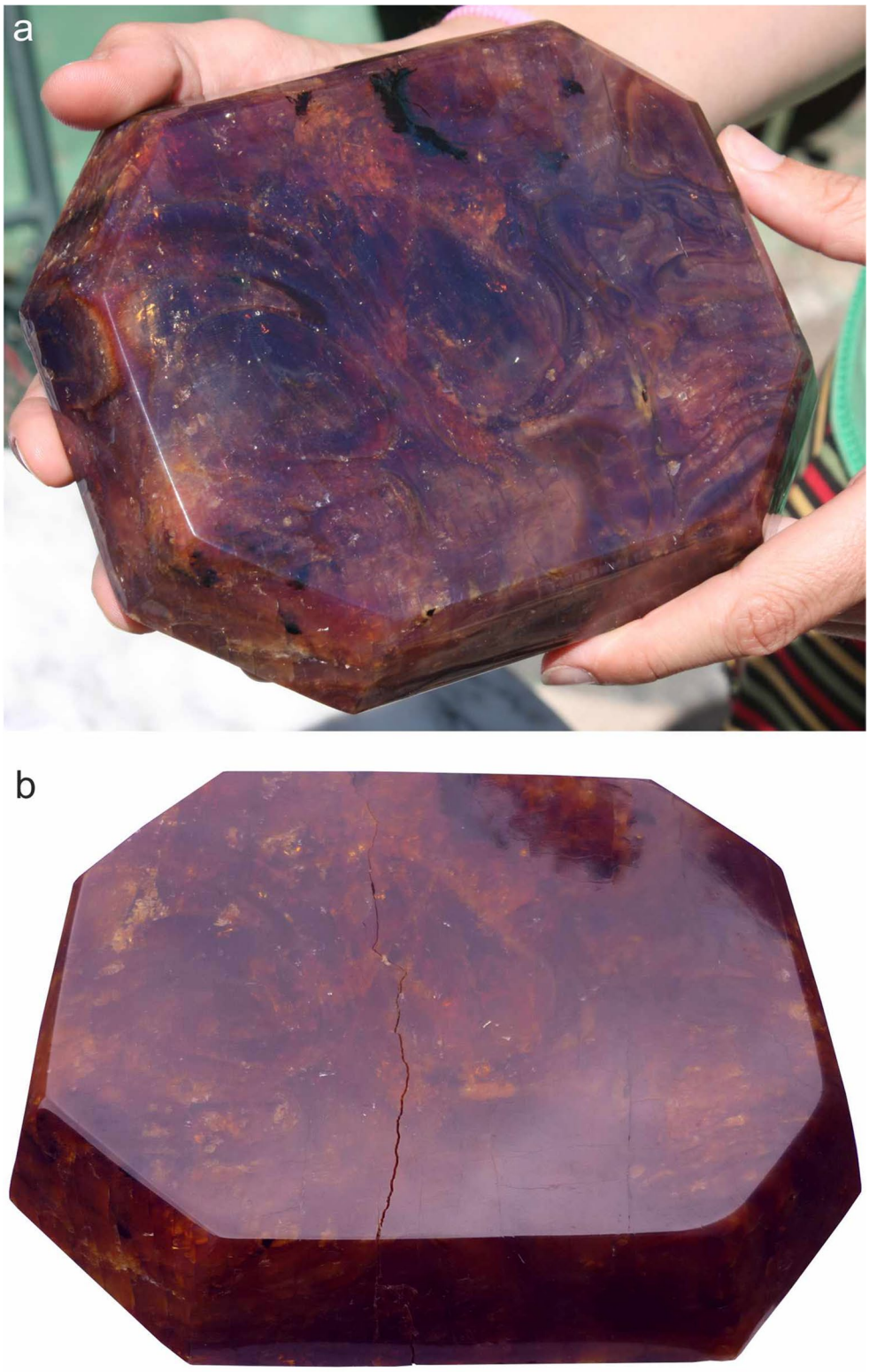

Fig. 6 Visible degradation in a faceted amber piece from Rábago-El Soplao. (**a**) Amber specimen (CES 318) faceted in 2010 by one of the authors (R.P.L.) from a kidney-shaped piece. The piece was carved on commission by the Government of Cantabria for the exhibition "The Long Journey of El Soplao Amber", which opened that same year. (**b**) Appearance of the specimen in 2023. Note the large crack running through the main face of the amber due to the formation of hydrated sulphates within it. Photographs were taken under the sunlight, bringing out some of the typical purple hue of the amber from this deposit

removal more challenging. For this reason, tests were carried out with amber and pyritised fossil molluscs exhibiting abundant efflorescence growth from Rábago-El Soplao. Although the material is very delicate, immersing the samples for 30 s in an ultrasonic tank followed by immersing them in commercial NC acetone 29,141,100 for quick drying is the most effective. This procedure successfully removes all halotrichite and a significant portion of the szomolnokite. The treatment is followed by applying a 3% ethanolamide thioglycolate solution in ethanol with a brush to neutralise the acid. Washing the samples with ethanol 24 h later, joining together the detached fragments of amber and pyrite and consolidating the whole piece using Fluoline (entirely reversible) complete the remedial procedure.

Discussion

The Pyritisation of Amber

To understand the deterioration of collections due to the oxidation/hydration of pyrite, it is essential to understand the textural relationships between the sulphide and the amber. Pyrite-rich rock remains can be adhered on the surface of the specimens (Fig. 2a, b), either filling their thin veins (Fig. 3a, b) or in the form of nodules (Fig. 3f). The presence of pyrite crystals embedded in a matrix rich in phyllosilicates and quartz adhered to the amber specimens, and the presence of Al, Si, K, and O, in addition to the S and Fe characteristic of the sulphide (Figs. 2 and 3), indicates the existence of a nanometric silicate interface (probably rich in phyllosilicates) between the pyrite crystals and the matrix. The formation of this interface could have a diagenetic origin, similar to that of the pyrites from the Cameros Basin (NE Spain), where an interface of quartz and phyllosilicates separating the pyrite crystals from the lutite matrix has also been found, in that case related to the interaction of fluids with the matrix (Alonso-Azcárate et al. 1999).

Namely in subaerial specimens (namely kidney-shaped and formed by the roots or in tree pockets), the pyrite-rich rock remains are always linked to the more or less thick, opaque crusts milky coffee brown in colour. These areas correspond to areas where resinicolous fungal mycelia grew inwards while the resin was still fresh (Speranza et al. 2015). Fungal colonisation is superficial or can penetrate completely into the interior of some of the specimens assessed. Although these fungi fed on the resin, their advance towards the core of the resin pieces preferentially followed darker bands rich in pseudoinclusions partly formed by (likely phloem) sap (Lozano et al. 2020). The interconnected network of fungal hyphae provides access for water into the amber, facilitating pyritisation, as demonstrated by the pyrite filling the cores of some hyphae (Speranza et al. 2010, 2015). Furthermore, Speranza et al. (2015) suggested that fungus-altered amber behaved more fragile than unaltered amber and was therefore more susceptible to degradation during diagenesis. The formation of cracks exclusively in fungus-altered zones of the amber (Fig. 3a, b) supports this and demonstrates the high fragility of the altered amber. The opening of these cracks could be due to tectonic or diagenetic causes, the contraction of the resin due to the loss of volatiles during the hardening process, or conversely, to the expansion of the resin volume due to new resin injections into its core (Speranza et al. 2015). The presence of abundant framboidal pyrite within the pyrite infilling these cracks (Fig. 3e) indicates that the cracks opened relatively early, as the formation of this type of pyrite also occurs very early in the presence of organic matter (Vietti et al. 2015). Considering this, the cracks formed shortly after the resin emissions had hardened superficially, probably when their core was still receiving injections of fresh resin. Shortly after the cracks opened, sediment entered into the resin emissions, where framboidal pyrite began to nucleate under reducing conditions related to oxygen consumption associated with the oxidation of organic matter or its microbial processing (Duverger et al. 2021). In later diagenetic stages, much larger euhedral pyrite crystals grew than the framboidal crystals, and their expansion may have contributed to further opening of the cracks.

The origin of the pyrite nodules (Figs. 3f and 10c) could be related to the filling of bioerosions or invertebrate pellets, although this requires further study.

Fig. 7 SEM images (backscattered electrons) of hydrated sulphates found in the raw amber collection from Rábago-El Soplao and EDX spot chemical analyses (yellow crosses) obtained for each. (**a**) Acicular (hairy appearance) crystals of halotrichite in sample SO-3. (**b**) Aggregates of hexagonal tabular coquimbite crystals in sample SO-5. (**c**) Cluster of hexagonal prismatic paracoquimbite crystals in sample SO-5. (**d**) Aggregates of tabular szomolnokite crystals in sample SO-8. (**e**) Rosette-like aggregates of laminated hexagonal ferricopiapite crystals in sample SO-6. (**f**) Radial aggregate of pseudohexagonal prismatic crystals of gypsum in sample SO-4

Sulphation of the Pyrite-Rich Rock

Hydrated iron sulphates are typical products of oxidation zones in pyrite-rich mineralisations (Buckby et al. 2003; Biagioni et al. 2020; Dimitrova et al. 2020) and are also found in coal mines, where pyrite is similarly abundant (Cotterell 2009; Kruszewski 2019). Although they are also common in fossil collections under unsuitable and even suitable museum conditions (Tacker 2020), only one case has been hitherto studied in amber collections (Sadowski et al. 2021). In this latter study, only szomolnokite was identified, formed under museum conditions with RH around

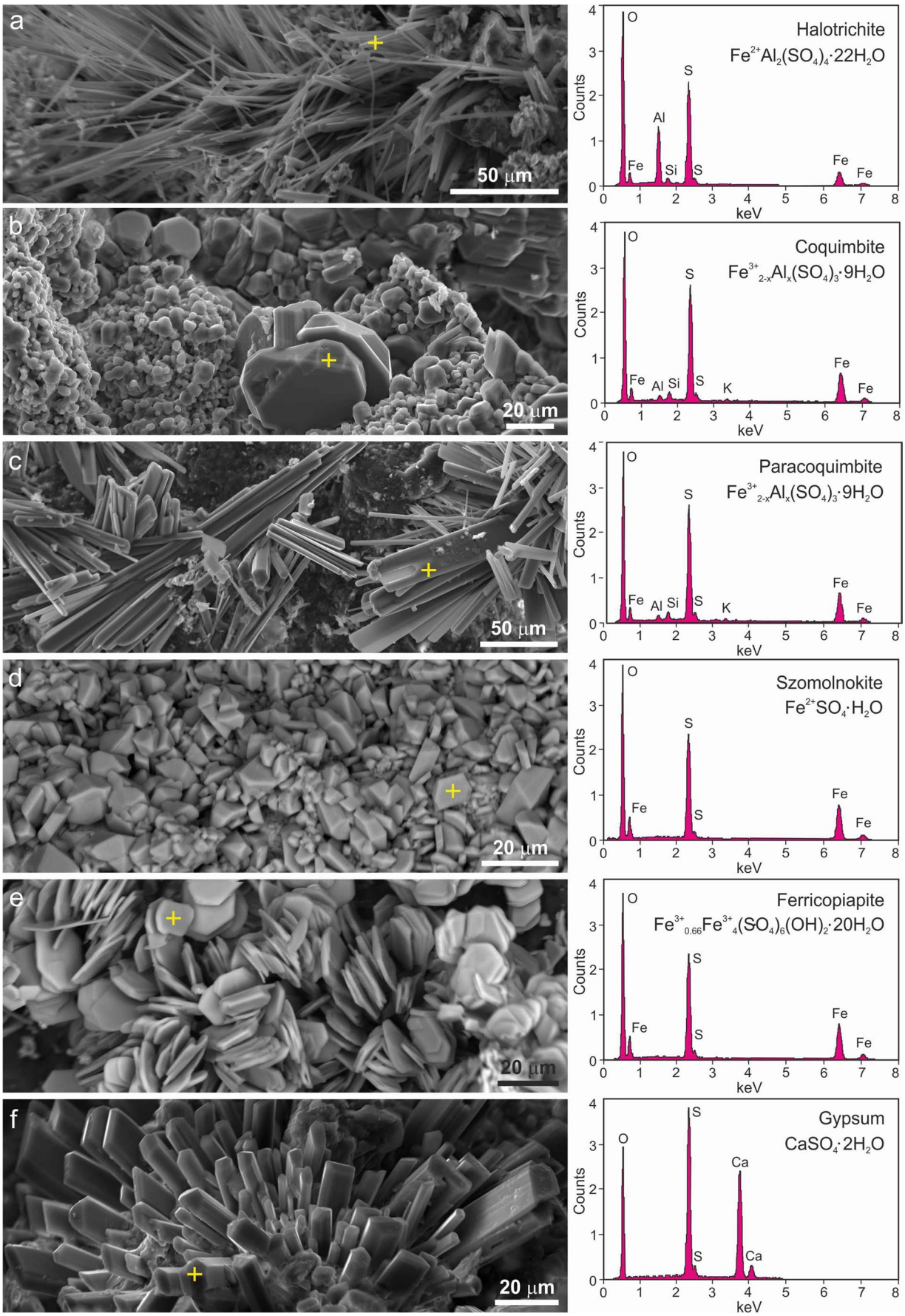
a
50 μm
Halotrichite
Fe2+Al2(SO4)4·22H2O
b
20 μm
Coquimbite
Fe3+2-xAlx(SO4)3·9H2O
c
50 μm
Paracoquimbite
Fe3+2-xAlx(SO4)3·9H2O
d
20 μm
Szomolnokite
Fe2+SO4·H2O
e
20 μm
Ferricopiapite
Fe3+0.66Fe3+4(SO4)6(OH)2·20H2O
f
20 μm
Gypsum
CaSO4·2H2O
Counts
keV
O
S
Al
Fe
Si
K
Ca

60%. The amber collections from Rábago-El Soplao have been preserved under high RH atmospheric conditions (with possible peaks of 100% RH), leading not only to the generation of szomolnokite efflorescences, but also other sulphates with more structural water, such as coquimbite and paracoquimbite (nine molecules of water), ferricopiapite (20 molecules of water), and halotrichite (22 molecules of water) (Fig. 7). With such a high amount of structural water, the volume increase is high relative to the initial volume of the pyrite-rich rock, rendering the deterioration severe. The order of sulphate crystallisation based on SEM observations is difficult to establish, as not all sulphates coexist in the same samples (Fig. 8), likely because they formed during different episodes coinciding with recurring condensation phases. However, it is probable that sulphates with a lower oxidation state (Fe^{2+}; halotrichite and szomolnokite) formed first, followed by sulphates with a higher oxidation state (Fe^{3+}; coquimbite, paracoquimbite, and ferricopiapite) as the former became exposed to the atmosphere (Wiese et al. 1987).

Although the efflorescences must have formed during several condensation/evaporation periods, no evidence of dissolution of any of the hydrated sulphates forming the efflorescences has been found in the studied samples, nor has the transition from one sulphate to another with different structural water content been observed. This is because sulphates form quickly but dehydrate very slowly (Tacker 2020). For this reason, amber efflorescences from Rábago-El Soplao commonly contain two sulphates with very different water contents, such as szomolnokite and halotrichite (Figs. 8 and 9), and ferricopiapite remains stable (Wang et al. 2012).

Another important factor to consider is the hygroscopicity of hydrated sulphates and clay minerals. Even if RH and T conditions do not cause condensation, once the sulphates have formed they can absorb water and transfer it to the pyrite surface. In this way, the chemical reaction involves not only RH and pyrite but also the hygroscopic sulphates themselves (Tacker 2020). The most extreme case is the early formation of amorphous sulphates, as they are even more hygroscopic than crystalline sulphates (Sklute et al. 2015, 2018). On the other hand, clays tend to be hygroscopic and can therefore retain water for extended periods after an increase and subsequent decrease in humidity. Thus, water would be more or less continuously available at potential reaction sites. In addition, clays can also conduct electrons for redox reactions, which can further accelerate the process (Wiese et al. 1987).

The formation of Fe-Al sulphates indicates that not only has pyrite altered, but other minerals must also be involved in the process as a source of Al. The most reasonable assumption is that the phyllosilicates in the pyrite-rich rock, or even the coatings of the euhedral pyrite crystals (Fig. 2d), are the source. Indeed, the formation of halotrichite, coquimbite, and paracoquimbite could be related to the partial dissolution of the clay fraction of the rock remains (which contains Al, Si, and K) due to the generation of acid during the oxidation of pyrite. In sample SO-7, Fe-Al sulphates (probably coquimbite) are located on the phyllosilicate aggregates (possibly kaolinite), while the Fe sulphate (szomolnokite) covers the surface of the pyrite (Fig. 10c, d). Furthermore, the growth of halotrichite between the pyrite crystals in sample SO-8 (Fig. 9c, d, e) suggests the occurrence of clay beneath this mineral. This source of Al has also been suggested by Kruszewski (2019) in the formation of hydrated sulphates in coal mines and by Wiese et al. (1987) in the formation of efflorescences in coal under unsuitable museum conditions. The formation of gypsum is sporadic (Fig. 6f) and is likely related to the dissolution of sedimentary calcite.

In thin veins filled with pyrite-rich rock, the alteration process seems to begin in the framboidal pyrite due to its small grain size (Fig. 10b). Indeed, the smaller the grain size, the more intense the oxidation process (Huggins et al. 1983),

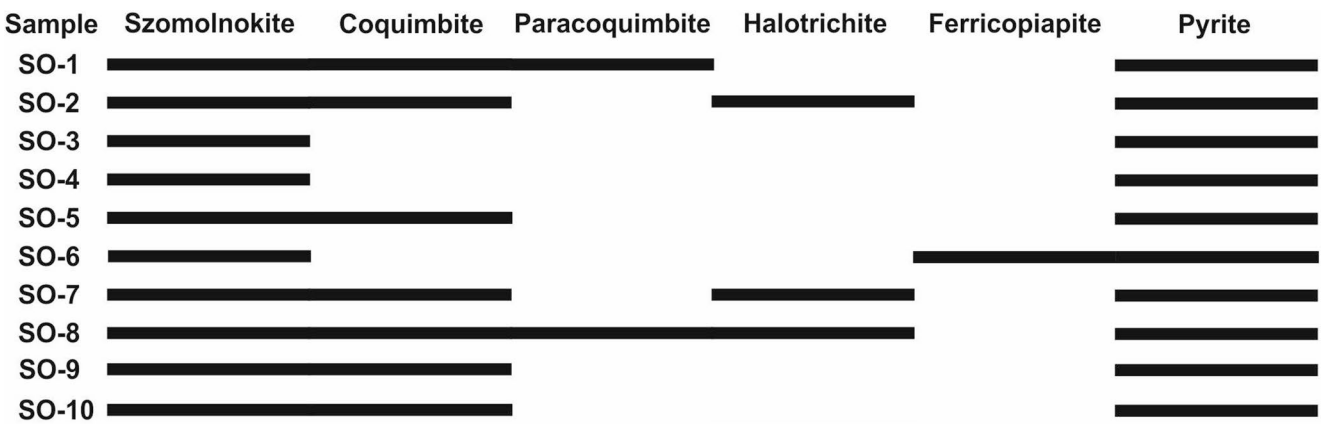

Fig. 8 Mineral determination by X-Ray Diffraction of the efflorescence samples studied herein

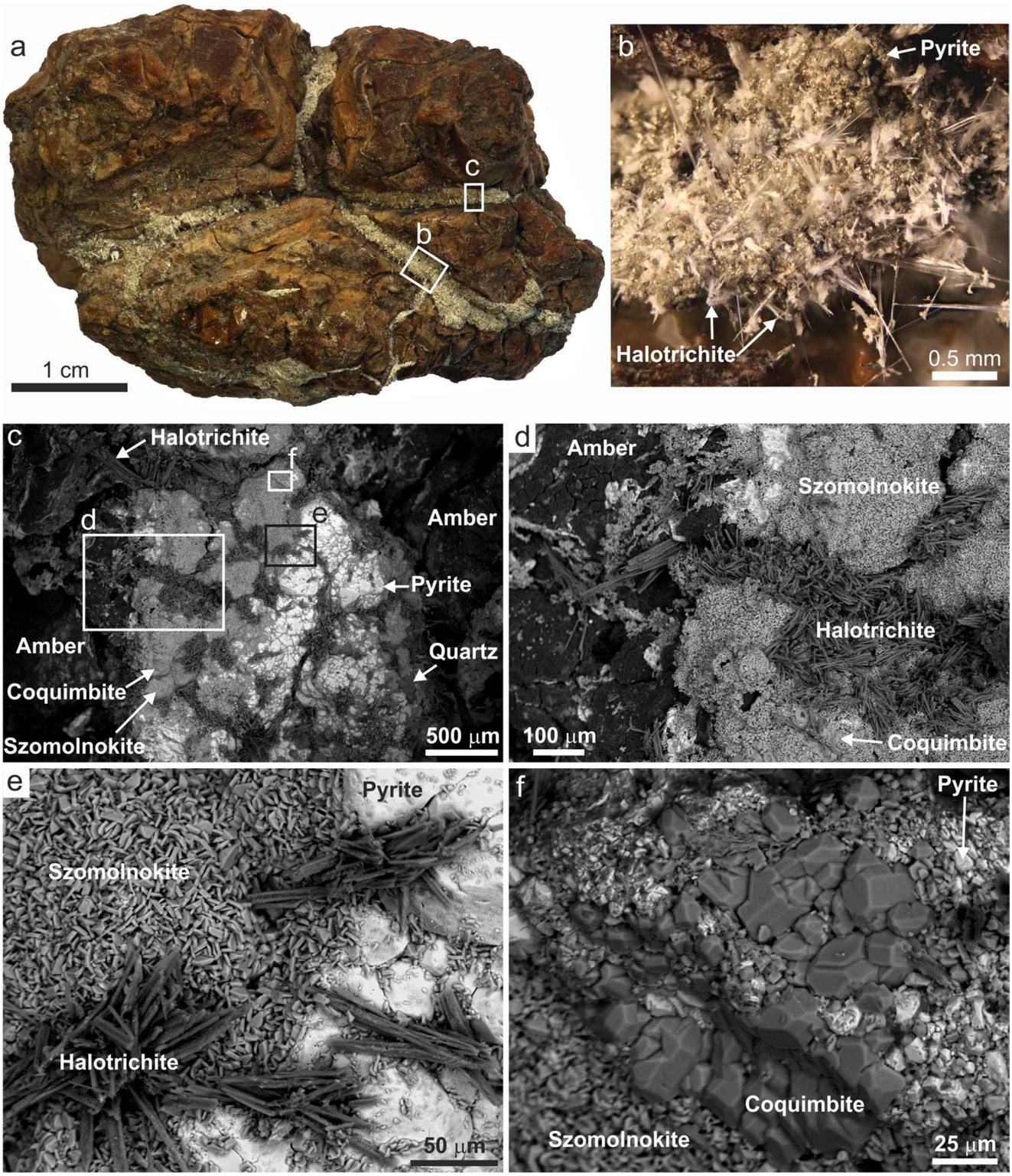

Fig. 9 Characterization of Rábago-El Soplao amber specimen with thin veins of pyrite-rich rock (sample SO-8) using macrophotography (**a**–**b**) and SEM images (backscattered electrons) (**c**–**f**). (**a**) General appearance of the sample, with efflorescences concentrated in small veins of pyrite-rich rock. (**b**) Detail from (**a**) of one of the veins with halotrichite growing (hairy in appearance) directly on pyrite. (**c**) Detail from (**a**) of another vein where pyrite-rich rock is partially covered by hydrated sulphates. (**d**) Detail from (**c**) of the vein edge. Szomolnokite and coquimbite partially cover the pyrite. Halotrichite grows in subcracks generated between the pyrite crystals. Note that the sulphate growth extends beyond the vein and into the amber. (**e**) Detail from (**c**) showing halotrichite growing between intercrystalline surfaces of pyrite and szomolnokite partially covering the sulphide. (**f**) Detail from (**c**) of coquimbite aggregates growing directly on pyrite. a–b: Obtained by stacking multiple images taken at different focal depths

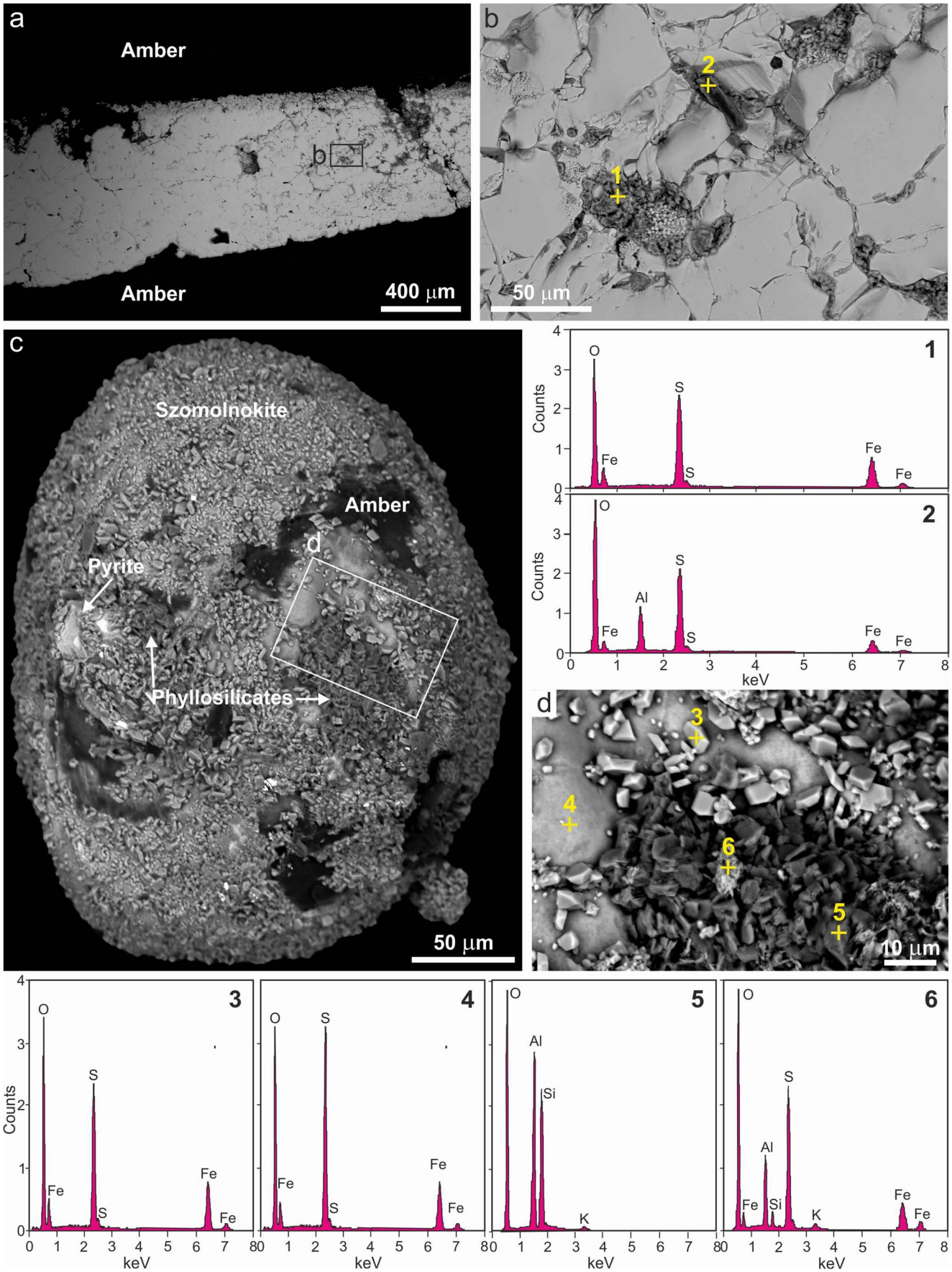
a
Amber
b
Amber
400 μm
b
2
1
50 μm
c
Szomolnokite
Amber
d
Pyrite
Phyllosilicates
50 μm
1
O
S
Fe
S
Fe
Fe
Counts
2
O
Al
S
Fe
S
Fe
Fe
Counts
keV
d
3
4
6
5
10 μm
3
O
S
Fe
S
Fe
Fe
Counts
4
O
S
Fe
S
Fe
Fe
5
O
Al
Si
K
6
O
S
Al
Fe
Si
K
Fe
Fe
keV

Fig. 10 Characterisation of fungus-altered Rábago-El Soplao amber using SEM (backscattered electrons) and EDX spot chemical analyses of hydrated sulphates. (**a**) Section of a pyrite-rich rocky vein within fungus-altered amber (sample SO-11; see Fig. 3a–b). Note that the right side of the vein is more fractured, with hydrated sulphates formed. (**b**) Detail from (**a**) showing preferential alteration of framboidal pyrite. Analysis 1 shows a Fe sulphate, probably szomolnokite; analysis 2 corresponds to a sulphate containing Fe and Al, probably halotrichite. (**c**) Pyrite-rich rock remain nodule extracted from within fungus-altered amber (sample SO-7; see Fig. 3f). Its surface is partially covered by hydrated sulphates and shows adhered remnants of fungus-altered amber and phyllosilicate patches. (**d**) Detail from (**c**): szomolnokite crystals (analysis 3) grow on an unidentified material (analysis 4), probably an amorphous iron sulphate, covering the pyrite. The phyllosilicate contains Al, Si, and O (with traces of K; analysis 5), suggesting it is kaolinite. A corroded-looking sulphate, probably coquimbite, is found on the kaolinite aggregate (analysis 6)

as the surface area exposed to water and oxygen is greater. The expansion due to the larger volume of sulphate relative to sulphide causes fracturing of the coarse-grained pyrite (using intercrystalline surfaces), where sulphates begin to grow, further expanding the cracks (Fig. 11a). This expansion of the veins causes the adjacent amber to fracture, which is very fragile due to fungal alteration, and these recent cracks are also filled with sulphates (Fig. 11b, c, d), further advancing the deterioration of the amber specimens. Like the rest of the pyrite, the replaced mollusc shells are also altered to sulphates (Fig. 12). In some cases, the growth of sulphates inside the fossils causes the expansion and fracturing of the replaced shell (Fig. 12d), further contributing to the increase in volume that leads to the fracturing of the amber. In the nodules, an amorphous sulphate appears to form directly on the pyrite before szomolnokite crystallisation (Fig. 10c, d), as observed by Wiese et al. (1987) in the formation of sulphates on coal under museum conditions. The growth of sulphates around the nodules produces the same expansive effect, culminating in the fracturing of the surrounding amber.

Preventive and Curative Recommendations

The presence of pyrite and clay-rich rock remains in specimens poses a significant challenge for the conservation of amber, adding this factor to the inherent risks and complexities associated with the organic nature of amber (e.g., Bisulca et al. 2012). Since the deterioration caused by pyrite alteration can become irreversible, it is highly advisable to establish a series of preventive measures to avoid such damage in the collection setting.

The most widely adopted procedure for mitigating pyrite efflorescence involves storing specimens in hermetically sealed containers under stable, dry conditions, with RH maintained below 30% (Howie 1992). However, in environments of such low humidity, amber is liable to undergo deterioration through dehydration (Howie 1995). On this basis, the optimal RH range for the preservation of such specimens is considered to lie between 35% and 45%. Nonetheless, oxidation continues to occur under conditions of reduced RH, as hygroscopic efflorescences and associated clays continue to transfer moisture to the pyrite; in addition, oxygen remains the principal oxidising agent (Tacker 2020). Consequently, specimens should be stored under anoxic conditions, i.e. in containers that have been vacuum-sealed or in which the ambient air has been replaced by an inert gas such as nitrogen or argon. Anoxic storage conditions are routinely employed in the preservation of organic materials including paper, textiles, and mummified remains, as they not only protect specimens from RH fluctuations and oxygen exposure, but also from all oxygen-dependent biological agents (Maekawa 1998). Tacker's (2020) recommendation to preserve specimens in impermeable plastic "balloons" filled with dry nitrogen and heat-sealed is the most effective approach. Such containers are relatively inexpensive, and their integrity can be verified through straightforward periodic inspection of the inflation.

Any raw specimens added to an amber collection should be thoroughly examined to identify traces of pyrite-rich sediments on their surface, with the goal of removing them. The challenge lies with specimens that contain thin veins or internal nodules. Because the crust of many amber specimens is opaque, the identification of pyrite-rich rock inclusions is practically impossible by optical methods. Qualitative density determination could be useful to verify whether the amber specimen contains pyrite-rich rock inclusions. The density of amber is around 1 g/cm^3 while the density of pyrite-rich rock is much higher (3–5 g/cm^3). When amber contains inclusions of pyrite-rich rock its density will be greater than 1 g/cm^3 and could be detected through a simple test by measuring buoyancy immersed in liquids of known density. Affectation by pyrite can also be assessed using X-rays, for instance through microtomography (CT-Scan).

Amber specimens to be polished and under the risk of pyrite affectation (excluding those containing bioinclusions) should be coated with a thin layer of transparent epoxy resin (0.5 mm would suffice). Such layer will protect the interior from oxygen and moisture ingress without substantially altering the appearance of the amber. The protection of amber specimens with epoxy resin (EPO-TEK 301) has proven effective, as demonstrated by the excellent preservation of sample 495 (Fig. 3e, f) 12 years after its preparation, and the pristine condition of sample 9935 from Peñacerrada (Álava, Spain) after almost 25 years.

Cracked polished material (Fig. 6b) should also be treated with epoxy resin to prevent further deterioration. Oxygen and water ingress promoting the formation of hydrated sulphates within polished pieces can be prevented by applying

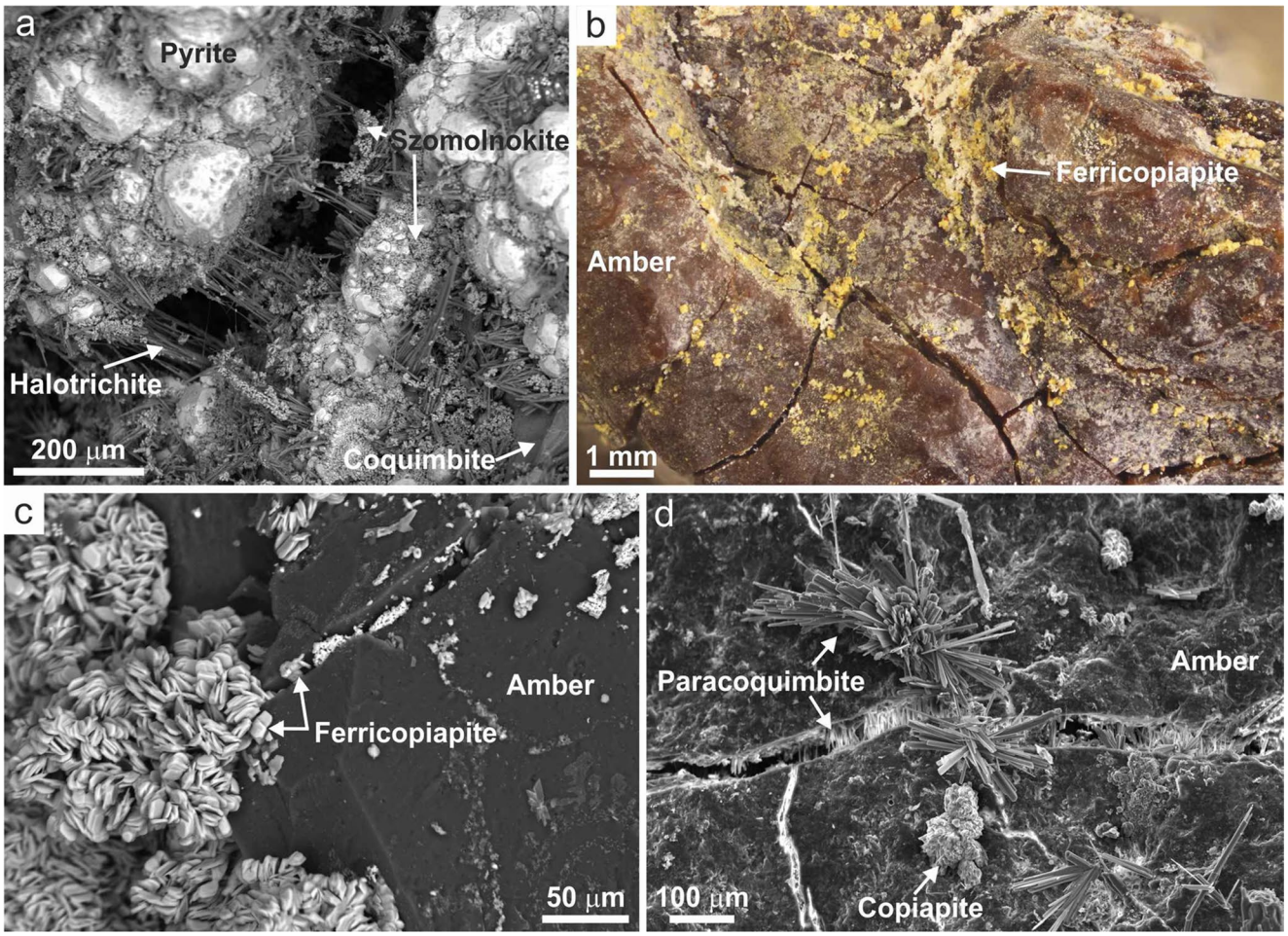

Fig. 11 Growth of hydrated sulphates in cracks and surfaces of Rábago-El Soplao amber. (**a**) Halotrichite and szomolnokite crystals in pyrite-rich sediment within a crack (sample SO-8; see Fig. 9a). (**b**) Ferricopiapite growth on the surface and in cracks formed in amber (sample SO-6). (**c**) Ferricopiapite growth in the cracks of the same sample. (**d**) Paracoquimbite growth on the surface and in a crack of amber (sample SO-5). a, c, d: SEM images. b: Macrophotograph obtained by stacking multiple images taken at different focal depths

epoxy resin in a vacuum chamber, which penetrates the cracks. The use of epoxy resin should not be limited to areas with visible cracks but also applied across the entire surfaces in order to seal fractures that are not visible to the naked eye.

Restoration of the amber specimens depends on their degree of alteration. Many have fragmented completely (Fig. 5a), rendering their reconstruction challenging. Specimens with a lower degree of alteration can be restored using various treatments described for fossils deteriorated by pyrite alteration, which include the neutralisation of acid and the removal of efflorescences (Larkin 2011). The tests performed on amber and pyritised fossil molluscs from Rábago-El Soplao recommend a similar procedure, starting with the removal of the efflorescences with ultrasound, followed by neutralisation with an alkaline solution and finished with consolidation using a reversible product.

Conclusions

The collection of raw and polished amber specimens from the Rábago-El Soplao locality (lacking bioinclusions) suffered significant deterioration due to the formation of hydrated sulphates, induced by the oxidation/hydration of pyrite-rich sediments associated with the amber pieces. The collection remained for nearly 10 years without proper monitoring in an uninsulated room where the average RH exceeds 75% and regular peaks at 100%.

Understanding the textural relationship between pyrite, the sedimentary rock, and amber is essential for elucidating the growth of efflorescences and the resulting deterioration of the amber specimens. Pyrite and remains of the amber-bearing rock may be adhered to the surface of the amber or within it as thin infilled veins or nodules, always in contact with areas of amber altered by the action of resinicolous fungi while the resin was still fresh.

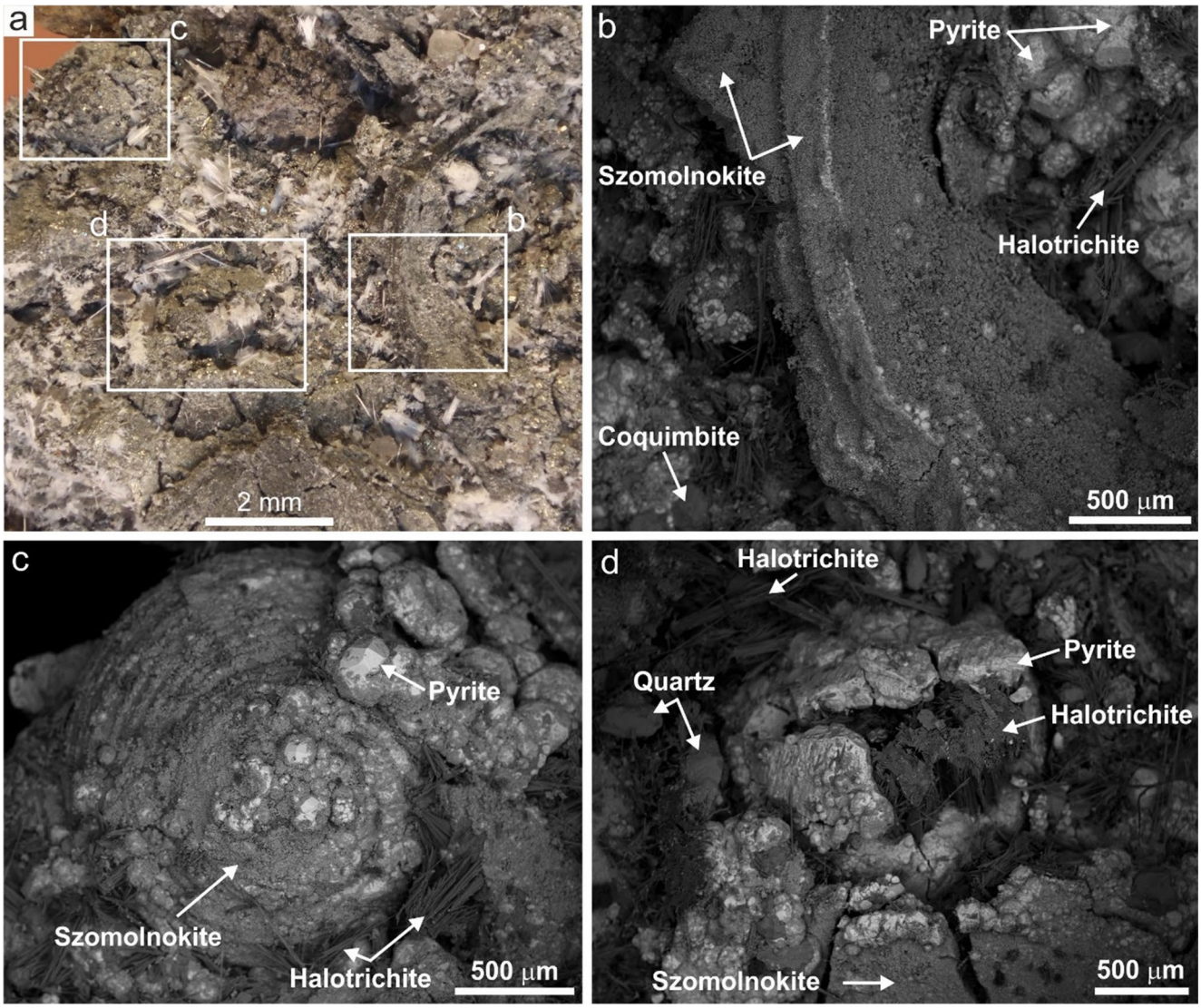

Fig. 12 Interior of a small pyrite-rich rock vein embedded in Rábago-El Soplao amber, (sample SO-8; see Fig. 7a). (**a**) Macrophotograph showing several mollusc shells replaced by pyrite and altered to sulphates. The most visible sulphates are halotrichite aggregates (white structures with a hairy appearance). Framed areas (**b**–**d**) correspond to SEM (backscattered electrons) images. Image obtained by stacking multiple images taken at different focal depths. (**b**) Detail of a pyritized shell fragment, probably from a bivalve. The sulphide is completely covered by small szomolnokite crystals. (**c**) Detail of a pyritized gastropod shell. Note the trapezohedral pyrite crystals, partially covered by szomolnokite. (**d**) Detail of an undifferentiated fossil remains (probably a gastropod), cracked by the growth of halotrichite inside

Sulphates with different structural water contents detected in the altered zones of the amber specimens most likely formed during several condensation/evaporation stages. The presence of Fe-Al sulphates with Si and K impurities suggests the partial dissolution of the clay of the rock within an acidic environment. Additionally, clays and sulphates can hygroscopically absorb water, accelerating the pyrite alteration process.

Initially, the growth of sulphates triggers the fracturing of the pyrite-rich rock. The generated fractures expand as the sulphates grow, eventually fracturing the adjacent amber, where sulphates also begin to grow, further expanding the fractures until the specimens disintegrate.

Preventative recommendations for amber collections against pyrite disease include storing the amber specimens in impermeable plastic “balloons” filled with dry nitrogen, and detecting pyrite inclusions through density testing. Additionally, polished specimens without bioinclusions should be coated with a layer of colourless epoxy resin to isolate them from oxygen and atmospheric water. Restorative recommendations include the cleaning both pyrite-rich rock remains and pyrite mineralisations adhered to the amber pieces, the removal of efflorescences using ultrasound, the alkaline neutralisation of acid, and the reconstruction/consolidation of the raw specimens employing reversible products.

The results of this research are not only relevant for the conservation of palaeontological amber collections but also for the preservation of amber in mineralogical, gemological, and archaeological collections. The future of the Rábago-El Soplao amber collection is at risk. It is necessary that this remarkable material, which has enabled high-level scientific production and has the potential to keep providing invaluable data on the terrestrial ecosystems from more than 100 million years ago, is secured under basic conditions that guarantee its preservation in time, which do not exist at present. The establishment of an uninterrupted conservator/curator post is essential to ensure the integrity of the collection and that it stays relevant for future generations.

Acknowledgements The authors thank Berta Ordoñez Casado for her assistance with the SEM work and Xoan Moreno Paredes for his comments on amber conservation. We greatly appreciate the constructive comments from Robert Christopher Tacker.

Author Contributions R.P.L. designed the project, gathered data and made the figures. R.P.L., R.-l.d.V and G.D. prepared the samples. R.P.L., R.-l.d.V, R.P.-d.l.F, E.B., G.D, A.R., E.P. and E.B. analyzed the data and contributed to the discussion. R.P.L., R.P.-d.l.F. and E.P. wrote the paper.

Funding Open Access funding provided thanks to the CRUE-CSIC agreement with Springer Nature. This work was primarily supported by the Consejería de Industria, Turismo, Innovación, Transporte y Comercio of the Gobierno de Cantabria through the semipublic enterprise EL SOPLAO S.L. (Ref. VAPC 20225428 of IGME, CSIC, for the period 2022–2025) and by the project PID2022-137316NB, funded by MICIU/AEI/https://doi.org/10.13039/501100011033 and by ERDF/EU.

Data Availability All the data necessary used in this paper is provided herein. There are no supplementary data.

Declarations

Conflict of interest The authors declare no conflict of interest to disclose.

References

Alonso-Azcárate J, Rodas M, Bottrell SH, Raiswell R, Velasco F, Mas JR (1999) Pathways and distances of fluid flow during low-grade metamorphism: evidence from pyrite deposits of the Cameros Basin, Spain. J Metamorph Geol 17:339–348. https://doi.org/10.1046/j.1525-1314.1999.00202.x

Álvarez-Parra S, Pérez-de la Fuente R, Peñalver E, Barrón E, Alcalá L, Pérez-Cano J, Martín-Closas C, Trabelsi K, Meléndez N, López D, Valle R, Lozano RP, Peris D, Rodrigo A, Sarto i Monteys V, Bueno-Cebollada CA, Menor-Salván C, Philippe M, Sánchez-García A, Peña-Kairath C, Arillo A, Espílez E, Mampel L, Delclòs X (2021) Dinosaur bonebed amber from an original swamp forest soil. Elife 10:e72477. https://doi.org/10.7554/eLife.72477

Álvarez-Parra S, Peñalver E, Nel A, Delclòs X (2023) Barklice (Insecta: Psocodea) from Early Cretaceous resiniferous forests of Iberia (Spanish amber): new Troctomorpha and a possible Psocomorpha. Cretac Res 148:105544. https://doi.org/10.1016/j.cretres.2023.105544

Arillo A, Peñalver E, Pérez-de la Fuente R, Delclòs X, Criscione J, Barden PM, Riccio ML, Grimaldi DA (2015) Long-proboscid brachyceran flies in cretaceous amber (Diptera: stratiomyomorpha: Zhangsolvidae). Syst Entomol 40:242–267. https://doi.org/10.1111/syen.12106

Arillo A, Subías LS, Sánchez-García A (2016) New species of fossil oribatid mites (Acariformes, Oribatida), from the lower cretaceous amber of Spain. Cretac Res 63:68–76. https://doi.org/10.1016/j.cretres.2016.02.009

Arillo A, Blagoderov V, Peñalver E (2018) Early cretaceous parasitism in amber: a new species of *Burmazelmira* fly (Diptera: Archizelmiridae) parasitized by a *Leptus* sp. mite (Acari, Erythraeidae). Cretac Res 86:24–32. https://doi.org/10.1016/j.cretres.2018.02.006

Baeza E, Lozano RP, de la Fuente M, Menéndez S, Peñalver E, Rodrigo A (2007) Proyecto de conservación preventiva y restauración de La colección de ámbar Del Museo geominero (Instituto Geológico y Minero de España). La conservación infalible, de La Teoría a La Realidad. Actas Del III congreso Español Del IIC. International Institute for Conservation of Historic and Artistic Works, pp 361–370

Becherini F, del Favero L, Fornasiero M, Guastoni A, Bernardi A (2018) Pyrite decay of large fossils: the case study of the hall of palms in Padova, Italy. Minerals 8:40. https://doi.org/10.3390/min8020040

Biagioni C, Mauro D, Pasero M (2020) Sulfates from the pyrite ore deposits of the Apuan Alps (Tuscany, Italy): a review. Minerals 10:1092. https://doi.org/10.3390/min10121092

Bisulca C, Nascimbene PC, Elkin L, Grimaldi DA (2012) Variation in the deterioration of fossil resins and implications for the conservation of fossils in amber. Am Mus Novit 3734:1–19. https://doi.org/10.1206/3734.2

Buckby T, Black S, Coleman ML, Hodson ME (2003) Fe-sulphate-rich evaporative mineral precipitates from the Río Tinto, Southwest Spain. Mineral Mag 67(2):263–278. https://doi.org/10.1180/0026461036720104

Cotterell TF (2009) A review of halotrichite group minerals in Wales. UK J Mines Min 30:43–47

Dimitrova D, Mladenova V, Hecht L (2020) Efflorescent sulfate crystallization on fractured and polished colloform pyrite surfaces: a migration pathway of trace elements. Minerals 10:12. https://doi.org/10.3390/min10010012

Duverger A, Bernard S, Viennet JC, Miot J, Busigny V (2021) Formation of pyrite spherules from mixtures of biogenic FeS and organic compounds during experimental diagenesis. Geochem Geophys Geosyst 22:e2021GC010056. https://doi.org/10.1029/2021GC010056

Girard V, Franz C, Solórzano Kraemer MM (2012) Management of the Senckenberg amber collection and research developments. Geol Curator 9(7):373–380. https://doi.org/10.55468/GC71

Hansen EF (1998) Protection of objects from environmental deterioration by reducing their exposure to oxygen. In: Maekawa S (Ed.)

Oxygen-free museum cases pp 7–15. https://www.getty.edu/conservation/publications_resources/pdf_publications/pdf/oxygenfree.pdf

Hartl C, Schmidt AR, Heinrichs J, Seyfullah LJ, Schafer N, Grohn C, Rikkinen J, Kaasalainen U (2015) Lichen preservation in amber: morphology, ultrastructure, chemofossils, and taphonomic alteration. Foss Rec 18:127–135. https://doi.org/10.5194/fr-18-127-2015

Heinrichs J, Vitt DH, Schafer-Verwimp A, Ragazzi E, Marzaro G, Grimaldi DA, Nascimbene PC, Feldberg K, Schmidt AR (2013) The moss *Macromitrium richardii* (Orthotrichaceae) with sporophyte and calyptra enclosed in *Hymenaea* resin from the Dominican Republic. Pol Bot J 58:221–230. https://doi.org/10.2478/pbj-2013-0022

Hellemond A (2019) The Dendermonde mammoth: fighting pyrite decay and the preservation of unique paleontological heritage. Geol Curator 11:55–59. https://doi.org/10.55468/GC408

Howie FMP (1992) The care and conservation of geological materials: minerals, rocks, meteorites and lunar finds. Butterworth-Heinemann, Oxford, England. https://doi.org/10.4324/9781315042626

Howie FMP (1995) Aspects of conservation of fossil resins and lignitic material. In: Collis C (ed) The care and conservation of palaeontological material. Butterworth & Heinemann, London, pp 47–52

Huggins FE, Huffman GP, Lin MC (1983) Observations on low-temperature oxidation of minerals in bituminous coals. Int J Coal Geol 3:157–182. https://doi.org/10.1016/0166-5162(83)90008-3

Kruszewski L (2019) Secondary sulphate minerals from Bhanine Valley coals (South Lebanon) – a crystallochemical and geochemical study. Geol Q 63(1):65–87. https://doi.org/10.7306/gq.1450

Larkin NR (2011) Pyrite decay: cause and effect, prevention and cure. NatSCA News 21:35–43

Lozano RP, de la Pérez Fuente R, Barrón E, Rodrigo A, Viejo JL, Peñalver E (2020) Phloem sap in Cretaceous ambers as abundant double emulsions preserving organic and inorganic residues. Sci Rep 10:9751. https://doi.org/10.1038/s41598-020-66631-4

Lukashevich ED, Arillo A (2016) New eoptychoptera (Insecta: Diptera, Ptychopteridae) from the lower cretaceous of Spain. Cretac Res 58:254–264. https://doi.org/10.1016/j.cretres.2015.10.013

Maekawa S (1998) Conservation of the Royal Mummy Collection at the Egyptian Museum. In: Maekawa S (Ed.) Oxygen-free museum cases pp 1–5. https://www.getty.edu/conservation/publications_resources/pdf_publications/pdf/oxygenfree.pdf

Martín-González A, Wierzchos J, Gutiérrez JC, Alonso J, Ascaso C (2009) Double fossilization in eukaryotic microorganisms from lower cretaceous amber. BMC Biol 7:1–11. https://doi.org/10.1186/1741-7007-7-9

Menor-Salván C, Najarro M, Velasco F, Tornos F, Rosales I (2009) A new lower cretaceous fossil resin from El Soplao, Cantabria (Spain): biomarkers and chemotaxonomy. Geochim Cosmochim Acta 73(13S):A870

Menor-Salván C, Najarro M, Velasco F, Rosales I, Tornos F, Simoneit BRT (2010) Terpenoids in extracts of lower cretaceous ambers from the Basque Cantabrian basin (El Soplao, Cantabria, Spain): paleochemotaxonomic aspects. Org Geochem 41(10):1089–1103. https://doi.org/10.1016/j.orggeochem.2010.06.013

Menor-Salván C, Simoneit BRT, Ruiz-Bermejo M, Alonso J (2016) The molecular composition of cretaceous ambers: identification and chemosystematic relevance of 1,6-dimethyl-5-alkyltetralins and related bisnorlabdane biomarkers. Org Geochem 93:7–21. https://doi.org/10.1016/j.orggeochem.2015.12.010

Najarro M, Peñalver E, Rosales I, Pérez-de la Fuente R, Daviero-Gomez V, Gomez B, Delclòs X (2009) Unusual concentration of early Albian arthropod-bearing amber in the Basque-Cantabrian basin (El Soplao, Cantabria, Northern Spain): palaeoenvironmental and palaeobiological implications. Geol Acta 7(3):363–387. https://doi.org/10.1344/105.000001443

Najarro M, Peñalver E, Pérez-de la Fuente R, Ortega-Blanco J, Menor-Salván C, Barrón E, Soriano C, Rosales I, López del Valle R, Velasco F, Tornos F, Daviero-Gomez V, Gomez B, Delclòs X (2010) Review of the El Soplao amber outcrop, early cretaceous of Cantabria, Spain. Acta Geol Sin 84(4):959–976. https://doi.org/10.1111/J.1755-6724.2010.00258.X

Ortega-Blanco J, Peñalver E, Delclòs X, Engel MS (2011a) False fairy wasps in early cretaceous amber from Spain (Hymenoptera: Mymarommatoidea). Palaeontology 54(3):511–523. https://doi.org/10.1111/j.1475-4983.2011.01049.x

Ortega-Blanco J, Delclòs X, Peñalver E, Engel MS (2011b) Serphitid wasps in Early Cretaceous amber from Spain (Hymenoptera: Serphitidae). Cretac Res 32:143–154. https://doi.org/10.1016/j.cretres.2010.11.004

Pastorelli G, Richter J, Shashoua Y (2011) Photoageing of Baltic amber – influence of daylight radiation behind window glass on surface colour and chemistry. Polym Degrad Stab 96:1996–2001. https://doi.org/10.1016/j.polymdegradstab.2011.08.013

Pastorelli G, Shashoua Y, Richter J (2013) Surface yellowing and fragmentation as warning signs of depolymerisation in Baltic amber. Polym Degrad Stab 98:2317–2322. https://doi.org/10.1016/j.polymdegradstab.2013.08.009

Peñalver E, Ortega J, Nel A, Delclòs X (2010) Mesozoic Evaniidae (Insecta: Hymenoptera) in Spanish amber: reanalysis of the phylogeny of the Evanioidea. Acta Geol Sin 84(4):809–827. https://doi.org/10.1111/j.1755-6724.2010.00257.x

Peñalver E, Arillo A, Riccio ML, Pérez-de la Fuente R, Delclòs X, Barrón E, Grimaldi DA (2015) Long-proboscid flies as pollinators of cretaceous gymnosperms. Curr Biol 25(14):1917–1923. https://doi.org/10.1016/j.cub.2015.05.062

Pérez-Castañeda T, Jiménez-Riobóo RJ, Ramos MA (2014) Two-level systems and boson peak remain stable in 110-Million-year-old amber glass. Phys Rev Lett 112:165901. https://doi.org/10.1103/PhysRevLett.112.165901

Pérez-de la Fuente R, Peñalver E (2019) A mantidfly in cretaceous Spanish amber provides insights into the evolution of integumentary specialisations on the raptorial foreleg. Sci Rep 9(1):13248. https://doi.org/10.1038/s41598-019-49398-1

de la Pérez- Fuente R, Delclòs X, Peñalver E, Arillo A (2011) Biting midges (Diptera: Ceratopogonidae) from the Early Cretaceous El Soplao amber (N Spain). Cretac Res 32:750–761. https://doi.org/10.1016/j.cretres.2011.05.003

Pérez-de la Fuente R, Peñalver E, Ortega-Blanco J (2012a) A new species of the diverse cretaceous genus *Cretevania* Rasnitsyn, 1975 (Hymenoptera: Evaniidae) from Spanish amber. Zootaxa 3514:70–78. https://doi.org/10.11646/zootaxa.3514.1.4

de la Pérez- Fuente R, Peñalver E, Delclòs X, Engel MS (2012b) Snakefly diversity in early Cretaceous amber from Spain (Neuropterida, Raphidioptera). ZooKeys 204:1–40. https://doi.org/10.3897/zookeys.204.2740

Pérez-de la Fuente R, Saupe EE, Selden PA (2013) New lagonomegopid spiders (Araneae: Lagonomegopidae) from early cretaceous Spanish amber. J Syst Palaeontol 11(5):531–553. https://doi.org/10.1080/14772019.2012.725679

de la Pérez- Fuente R, Delclòs X, Peñalver E, Engel MS (2016) A defensive behavior and plant-insect interaction in cretaceous amber - the case of *Hallucinochrysa diogenesi*. Arthropod Struct Dev 45(2):133–139. https://doi.org/10.1016/j.asd.2015.08.002

de la Pérez- Fuente R, Peñalver E, Engel MS (2021) Beaded lacewings (Neuroptera: Berothidae) in amber from the Lower Cretaceous of Spain. Cretac Res 119:104705. https://doi.org/10.1016/j.cretres.2020.104705

Peris D, Chatzimanolis S, Delclòs X (2014) Diversity of rove beetles (Coleoptera: Staphylinidae) in early cretaceous Spanish amber. Cretac Res 48:85–95. https://doi.org/10.1016/j.cretres.2013.11.008

Peris D, Peñalver E, Delclòs X, Barrón E, Pérez-de la Fuente R, Labandeira CC (2017) False blister beetles and the expansion of gymnosperm–insect pollination modes before angiosperm dominance. Curr Biol 27(6):897–904. https://doi.org/10.1016/j.cub.2017.02.009

Rossi C, Bajo P, Lozano RP, Hellstrom J (2018) Younger Dryas to early holocene paleoclimate in Cantabria (NS pain): constraints from speleothem Mg, annual fluorescence banding and stable isotope records. Quat Sci Rev 192:71–85. https://doi.org/10.1016/j.quascirev.2018.05.025

Sadowski EM, Schmidt AR, Seyfullah LJ, Solorzano-Kraemer MM, Neumann C, Perrichot V, Hamann C, Milke R, Nascimbene PC (2021) Conservation, preparation and imaging of diverse ambers and their inclusions. Earth-Sci Rev 220:103653. https://doi.org/10.1016/j.earscirev.2021.103653

Saupe EE, Pérez-de la Fuente R, Selden PA, Delclòs X, Tafforeau P, Soriano C (2011) New *Orchestina* Simon, 1882 (Araneae: Oonopidae) from cretaceous ambers of Spain and france: first spiders described using phase-contrast X-ray synchrotron microtomography. Palaeontology 55(1):127–143. https://doi.org/10.1111/j.1475-4983.2011.01123.x

Seyfullah LJ, Schmidt AR (2015) Fossil focus: stuck in time – life trapped in amber. Palaeontology Online 5(12):1–11. https://www.palaeontologyonline.com/?p=3822

Sklute EC, Jensen HB, Rogers AD, Reeder RJ (2015) Morphological, structural, and spectral characteristics of amorphous iron sulfates. J Geophys Res Planet 120:809–830. https://doi.org/10.1002/2014je004784

Sklute EC, Rogers AD, Gregerson JC, Jensen HB, Reeder RJ, Dyar MD (2018) Amorphous salts formed from rapid dehydration of multicomponent chloride and ferric sulfate brines: implications for Mars. Icarus 302:285–295. https://doi.org/10.1016/j.icarus.2017.11.018

Soszyńska-Maj A, Krzemińska E, Pérez-de la Fuente R, Wang JS, Szpila K, Skibińska K, Kopeć K, Krzemiński W (2022) Evolution of sexual conflict in scorpionflies. eLife 11:e70508. https://doi.org/10.7554/eLife.70508

Speranza M, Wierzchos J, Alonso J, Bettucci L, Martín-González A, Ascaso C (2010) Traditional and new microscopy techniques applied to the study of microscopic fungi included in amber. In: Méndez-Vilas A, Díaz J (eds) Microscopy: Science, Technology, applications and education. Formatex Research Center, pp 1135–1145

Speranza M, Ascaso C, Delclòs X, Peñalver E (2015) Cretaceous mycelia preserving fungal polysaccharides: taphonomic and paleoecological potential of microorganisms preserved in fossil resins. Geol Acta 13(4):363–385. https://doi.org/10.1344/GeologicaActa2015.13.4.8

Tacker RC (2020) A review of pyrite disease for paleontologists, with potential focused interventions. Pal Electron 23(3):a45. https://doi.org/10.26879/1044

Thickett D, Cruickshank P, Ward C (1995) The conservation of amber. Stud Conserv 40(4):217–226. https://doi.org/10.2307/1506496

Vietti LA, Bailey JV, Fox DL, Rogers RR (2015) Rapid formation of framboidal sulfides on bone surfaces from a simulated marine carcass fall. Palaios 30(4):327–334. https://doi.org/10.2110/palo.2014.027

Waddington J, Fenn J (1988) Preventive conservation of amber: some preliminary investigations. Collec Forum 4(2):25–31. https://spnhc.org/resources/4-2/

Wang AA, Ling ZC, Freeman JJ, Kong WG (2012) Stability field and phase transition pathways of hydrous ferric sulfates in the temperature range 50 degrees C to 5 degrees C: implication for Martian ferric sulfates. Icarus 218:622–643. https://doi.org/10.1016/j.icarus.2012.01.003

Wiese RG, Powell MA, Fyfe WS, Williams SR, Waddington JB, Fenn J (1987) Spontaneous formation of hydrated iron sulfates on laboratory samples of pyrite- and marcasite-bearing coals. Chem Geol 63:29–38. https://doi.org/10.1016/0009-2541(87)90071-4

Williams SR, Waddington JB, Fenn J (1990) Infrared spectroscopic analysis of central and South American amber exposed to air pollutants, biocides, light and moisture. Collec Forum 6(2):1–14